

# WW CROSS-SECTIONS AND DISTRIBUTIONS

*Conveners:* W. Beenakker and F.A. Berends

*Working group:* E.N. Argyres, D. Bardin, A. Denner, S. Dittmaier, J. Hoogland, S. Jadach, R. Kleiss, Y. Kurihara, D. Lehner, G. Montagna, T. Muehisa, O. Nicrosini, T. Ohl, G.J. van Oldenborgh, C.G. Papadopoulos, G. Passarino, F. Piccinini, B. Pietrzyk, T. Riemann, Y. Shimizu, M. Skrzypek

arXiv:hep-ph/9602351v1 20 Feb 1996

## Contents

<b>1</b>	<b>Introduction</b>	<b>3</b>
1.1	Goals of W-pair production . . . . .	3
1.1.1	Measurement of the mass of the W boson . . . . .	3
1.1.2	Test of non-abelian couplings . . . . .	4
1.2	How to obtain accurate predictions? . . . . .	5
<b>2</b>	<b>On-Shell W-Pair Production and W Decay</b>	<b>6</b>
2.1	Notation and conventions . . . . .	7
2.2	Lowest order . . . . .	10
2.3	Radiative corrections . . . . .	12
2.3.1	Radiative electroweak $\mathcal{O}(\alpha)$ corrections . . . . .	13
2.3.2	Approximations in the LEP2 region . . . . .	17
2.3.3	Higher-order corrections . . . . .	19
2.4	The width of the W boson . . . . .	25
2.4.1	The W-boson width in lowest order . . . . .	25
2.4.2	Higher-order corrections to the W-boson width . . . . .	26

<b>3</b>	<b>Off-Shell W-Pair Production</b>	<b>27</b>
3.1	Lowest order: an introduction . . . . .	28
3.2	Semi-analytical approach . . . . .	29
3.3	Lowest order: the gauge-invariance issue . . . . .	32
3.4	Radiative corrections . . . . .	37
3.4.1	Initial-state radiation . . . . .	38
3.4.2	The Coulomb singularity . . . . .	39
3.4.3	The hard-photon process . . . . .	41
3.4.4	General approach to radiative corrections within the pole scheme . . . . .	45
3.5	Reconnection effects . . . . .	46
<b>4</b>	<b>Concluding Remarks</b>	<b>48</b>
<b>A</b>	<b>Various Methods of Calculating QED Corrections</b>	<b>49</b>
A.1	The structure-function method . . . . .	49
A.2	The parton-shower method . . . . .	54
A.3	YFS exponentiation . . . . .	55

# 1 Introduction

## 1.1 Goals of W-pair production

The measurements performed at LEP1 have provided us with an extremely accurate knowledge of the parameters of the Z gauge boson: its mass, partial widths, and total width. Except perhaps for the  $b\bar{b}$  and  $c\bar{c}$  decay widths all data are in perfect agreement with the Standard-Model [1] (SM) predictions [2, 3]. There even is first evidence that the contributions of gauge-boson loops to the gauge-boson self-energies are indeed required [4]. Thus an indirect confirmation of the existence of the triple gauge-boson couplings (TGC's) has been obtained.

The future measurements of W-pair production at LEP2 will add two important pieces of information to our knowledge of the SM. One is a determination of the W mass, which at present is only directly measured at hadron colliders. The envisaged precision of 40–50 MeV gives a significant improvement on the present Tevatron measurements [5]. Since the W mass is one of the key parameters of the electroweak theory, such an improved accuracy makes the tests on the SM more stringent.

The second piece of information that W-pair production can provide is the structure of the triple gauge-boson couplings. These couplings now play a role in the tree-level cross-section, in contrast to LEP1 physics where they only enter through loop corrections. So the Yang-Mills character of the TGC's can be established by studying W-pair differential cross-sections at LEP2 energies. Since these couplings are at the heart of the non-abelian gauge theories, this information is essential for a direct confirmation of the SM.

### 1.1.1 Measurement of the mass of the W boson

With the precise measurement of the mass of the W boson at LEP2 the situation for the electroweak input parameters changes with respect to LEP1. The common practice at LEP1 [6] is to use for  $M_W$  a value derived from the Fermi constant  $G_\mu$ , which is accurately known from muon decay. The relation to obtain  $M_W$  follows from the SM prediction for muon decay

$$G_\mu = \frac{\alpha\pi}{\sqrt{2} M_W^2 (1 - M_W^2/M_Z^2)} \frac{1}{1 - \Delta r}, \quad (1)$$

where  $\Delta r = 0$  at tree level and where  $\Delta r$  is  $m_t$ - and  $M_H$ -dependent when loop corrections are included. Thus,  $M_W$  in LEP1 calculations is  $m_t$ - and  $M_H$ -dependent through the above procedure. At LEP2, where one wants to measure  $M_W$  and, hence, wants to treat  $M_W$  as a fit parameter, the above relation now primarily acts as a test of the SM. The above relation predicts for any chosen  $M_H$  and measured  $M_W$  a value for  $m_t$  that can be used as input for LEP2 loop calculations and can also be compared with the directly observed top-quark mass from the Tevatron [7].

As to the actual procedure to measure  $M_W$  from W-pair production, two methods are advocated [8]. A third one, involving the measurement of the endpoint energy of a charged lepton originating from a decaying W boson, was suggested a few years ago but turns out to be less promising than other methods.

One procedure requires a measurement of the total W-pair cross-section close to threshold, where the size of  $\sigma_{\text{tot}}$  is most sensitive to the W mass. The energy proposed is 161 GeV. For this method the theory should obviously predict  $\sigma_{\text{tot}}$  with a sufficient accuracy, to wit  $\sim 2\%$ .<sup>a</sup> Therefore the radiative corrections (RC's) to the total cross-section should be under control.

The other method looks at the decay products of the W bosons, in particular at the four- and two-jet production. From the measured momenta of the decay products one tries to reconstruct the W mass. In this reconstruction a good knowledge of the W-pair centre-of-mass energy is essential. Since there will be an energy loss due to initial-state radiation (ISR) of primarily photons, the W-pair energy will be different from the laboratory energy of the incoming electrons and positrons. So, for this method the ISR should be well under control, i.e. the theoretical error on the average energy loss,  $\langle E_\gamma \rangle = \int dE_\gamma (d\sigma/dE_\gamma) E_\gamma / \sigma_{\text{tot}}$ , should be less than 30 MeV, which translates into a theoretical error of less than 15 MeV on the reconstructed W mass. This again is an aspect of radiative corrections.

### 1.1.2 Test of non-abelian couplings

Within the SM the triple gauge-boson couplings have the Yang-Mills (YM) form. Amongst others, this specific form for the TGC's leads to a proper high-energy behaviour of the W-pair cross-section and is a requirement for having a renormalizable theory. Couplings different from the YM form, called anomalous or non-standard couplings, will in general lead to a high-energy behaviour of cross-sections increasing with energy and thereby violating unitarity. At LEP2 the energy is too low to see such effects and in order to establish the presence of anomalous couplings one therefore has to study in detail the angular distributions of the W bosons and their decay products. In particular, the angular distribution in the W-production angle  $\theta$  is sensitive to non-standard couplings. Again, the knowledge of RC's to the tree level SM predictions is required, since they affect the Born-level angular distributions [9].

As elsewhere in this volume a detailed report on non-standard TGC's is given [10], only a few comments will be made here.

When one considers the most general coupling between three gauge bosons allowed for by Lorentz invariance, assuming the gauge bosons to be coupled to conserved currents, one ends up with seven possible couplings for the ZWW and  $\gamma$ WW interaction. Of these seven there are three which are CP violating and one which is CP conserving but C and P violating [11].

---

<sup>a</sup>Throughout this report the required theoretical accuracy is taken to be half the expected statistical error.

In practice it will be impossible to set limits on all these couplings. Therefore usually some assumptions are made to reduce the number of 14 couplings [11, 12]. For instance, one may restrict oneself to CP-conserving non-standard couplings so that 8 couplings are left. Of these the electromagnetic ones can be reduced further by omitting the C and P violating one and requiring the strength of the electromagnetic coupling to be determined by the charge. Two possible anomalous electromagnetic couplings remain and four ZWW anomalous couplings. Even with this reduced number it will be impossible to set experimental limits on all of them simultaneously.

However, there are theoretical arguments that such a purely phenomenological approach is also not required. First of all one might use symmetry arguments, motivated by specific models for the non-standard physics, to find relations between the anomalous couplings [12]. Alternatively, when one considers the electroweak theory as an effective theory originating from a field theory that manifests itself at higher energies, then also some small anomalous couplings may be present at lower energies. In such a  $SU(2) \times U(1)$  gauge-invariant framework the non-standard physics, situated at an energy scale  $\Lambda$ , decouples at low energies and the anomalous TGC's are suppressed by factors  $(E/\Lambda)^{d-4}$ , according to the dimension ( $d$ ) of the corresponding operators. This naturally introduces a hierarchy amongst the anomalous TGC's based on the dimension of the corresponding operators [13].

From the perspective of this report the origin of the non-standard couplings is not so important, but the fact that they often modify angular distributions is relevant. Also SM effects – like RC's, the finite decay width of the W bosons, and background contributions – provide deviations from the tree-level distributions [9, 10].

## 1.2 How to obtain accurate predictions?

In order to extract the wanted information from W-pair production it is clear from the remarks above that RC's are needed for total and differential cross-sections and, moreover, for the determination of the energy loss. Anticipating  $\sim 10^4$  W-pair events, the theoretical accuracy that should be targeted for the SM predictions is  $\sim 0.5\%$ , although specific final states, distributions, or observables in fact often do not require such a precision (like, e.g.,  $\sigma_{\text{tot}}$  at 161 GeV or the energy loss).

Ideally one would like to have the full RC's to the final state of four fermions, which originate from the two decaying vector bosons. In practice such a very involved calculation does not exist and is hopefully not required in its complete form for the present accuracy. For the discussion of the LEP2 situation and strategy it is useful to distinguish three levels of sophistication in the description of W-pair production.

The first level is to consider on-shell W-pair production,  $e^+e^- \rightarrow W^+W^-$ , which at tree level is described by three diagrams: neutrino exchange in the  $t$  channel, and  $\gamma$  and Z exchange in the  $s$  channel. Here the complete  $\mathcal{O}(\alpha)$  RC's are known, comprising the virtual one-loop

corrections and the real-photon bremsstrahlung [14, 15]. When one wants to divide the  $\mathcal{O}(\alpha)$  corrections into different parts the situation differs from LEP1 [9].

As to the bremsstrahlung, a gauge-invariant separation into initial-state radiation, final-state radiation (FSR), and its interference is not possible like, e.g., in  $\mu$ -pair production at LEP1. The reason is that the photon should couple to all charged particles in a line of the Feynman diagram. The  $t$ -channel diagram then makes a separation into ISR and FSR impossible. However, the leading logarithmic (LL) part of ISR is in itself gauge-invariant. This can be combined with the LL QED virtual corrections so that a LL description with structure functions for ISR can be given [16].

A separation of the virtual corrections into a photonic and weak part is also not possible since charged vector bosons are already present at Born level, necessitating an interplay between  $\gamma$ - and Z-exchange diagrams in order to preserve  $SU(2)$  gauge invariance.

Once one has a description of on-shell W-pair production one can attach to it the on-shell W decay. Again, the RC's to this decay are known [17]–[20].

The next level of sophistication is to consider off-shell production of W pairs, which then decay into four fermions [21]. The W propagators with energy-dependent widths can be taken into account. Although this description of four-fermion production through virtual W bosons is a natural extension of the on-shell evaluation, it is not a gauge-invariant treatment. In fact there are more diagrams needed to calculate such a four-fermion process. As to RC's, the ISR and FSR can be implemented in LL approximation, but the full set of virtual corrections have not yet been calculated.

The final level for the study of W-pair production would be a full  $\mathcal{O}(\alpha)$ -corrected evaluation of all possible four-fermion final states. At tree level there now exist evaluations where, besides the three off-shell W-pair diagrams, all other diagrams for a specific four-fermion final state have been included [22]. On top of that ISR can be taken into account. Again, one has to be aware of possible gauge-invariance problems. In particular, the introduction of energy-dependent widths in the W-propagators will destroy electromagnetic gauge invariance and may introduce dramatically wrong cross-sections in certain regions of phase space.

As long as a full  $\mathcal{O}(\alpha)$ -corrected evaluation of four-fermion production is not available, certain approximative schemes, like for instance the ‘pole scheme’ [23]–[25], may be useful. This goes beyond the treatments where only ISR through structure functions is taken into account. Actual numerical results from a complete ‘pole-scheme’ evaluation are not yet available.

## 2 On-Shell W-Pair Production and W Decay

Although the actual process that will be probed at LEP2 is  $e^+e^- \rightarrow 4f(\gamma, g)$ , we first focus on the production and subsequent decay of on-shell W bosons, being basic building blocks in some of the schemes for handling off-shell W bosons. In contrast to off-shell W-pair production the

on-shell processes are not plagued by the problem of gauge invariance for unstable particles and a complete set of  $\mathcal{O}(\alpha)$  radiative corrections is available. Consequently, they are well suited for studying the typical sizes of various radiative corrections. Moreover, many of the important features of the production and decay of off-shell W bosons are already contained in the on-shell limit. We indicate explicitly where the width of the W bosons radically changes the on-shell predictions.

## 2.1 Notation and conventions

We use the Björken–Drell metric  $g_{\mu\nu} = \text{diag}(+1, -1, -1, -1)$  and fix the totally antisymmetric tensor by  $\epsilon^{0123} = +1$ . The matrix  $\gamma_5$  is defined as  $\gamma_5 = i\gamma^0\gamma^1\gamma^2\gamma^3$  and the helicity projectors  $\omega_{\pm}$ , which are used to project on right- and left-handed massless fermions, as

$$\omega_{\pm} = \frac{1}{2}(1 \pm \gamma_5). \quad (2)$$

First we set the conventions for the process

$$e^+(p_+, \kappa_+) + e^-(p_-, \kappa_-) \rightarrow W^+(k_+, \lambda_+) + W^-(k_-, \lambda_-), \quad (3)$$

where the arguments indicate the momenta and helicities of the incoming fermions and outgoing bosons ( $\kappa_i = \pm\frac{1}{2}$ ,  $\lambda_i = 1, 0, -1$ ). Note that we sometimes use the shorthand version  $\kappa_i = \pm$  in certain sub- and superscripts. In the centre-of-mass (CM) system of the  $e^+e^-$  pair, which we will refer to as the laboratory (LAB) system in the following, the momenta read

$$p_{\pm}^{\mu} = E(1, 0, 0, \mp 1), \quad k_{\pm}^{\mu} = E(1, \mp\beta \sin \theta, 0, \mp\beta \cos \theta), \quad (4)$$

with  $E$  denoting the beam energy,  $\theta$  the scattering angle between the  $e^+$  and the  $W^+$ , and  $\beta = \sqrt{1 - M_W^2/E^2}$  the velocity of the W bosons. The Mandelstam variables used in the following are given by

$$\begin{aligned} s &= (p_+ + p_-)^2 = (k_+ + k_-)^2 = 4E^2, \\ t &= (p_+ - k_+)^2 = (p_- - k_-)^2 = -E^2(1 + \beta^2 - 2\beta \cos \theta), \\ u &= (p_+ - k_-)^2 = (p_- - k_+)^2 = -E^2(1 + \beta^2 + 2\beta \cos \theta). \end{aligned} \quad (5)$$

In order to define helicity amplitudes we need to introduce the corresponding polarization vectors for the  $W^+$  and  $W^-$  boson<sup>b</sup>

$$\varepsilon_{\pm}^{\mu}(k_{\pm}, +1) = \frac{1}{\sqrt{2}}(0, \mp \cos \theta, -i, \pm \sin \theta),$$

---

<sup>b</sup>Note that the helicity of the massive W bosons is not Lorentz-invariant. We define it in the LAB system.

$$\begin{aligned}
\varepsilon_{\pm}^{\mu}(k_{\pm}, -1) &= \frac{1}{\sqrt{2}}(0, \mp \cos \theta, +i, \pm \sin \theta), \\
\varepsilon_{\pm}^{\mu}(k_{\pm}, 0) &= \frac{E}{M_W}(\beta, \mp \sin \theta, 0, \mp \cos \theta).
\end{aligned}
\tag{6}$$

Because we are neglecting the electron mass, the helicity of the positron is opposite to the helicity of the electron

$$\kappa_- = -\kappa_+ = \kappa. \tag{7}$$

Henceforth we refer to the helicity amplitudes for W-pair production as  $\mathcal{M}(\kappa, \lambda_+, \lambda_-, s, t)$ . CP invariance implies the relation:

$$\mathcal{M}(\kappa, \lambda_+, \lambda_-, s, t) = \mathcal{M}(\kappa, -\lambda_-, -\lambda_+, s, t). \tag{8}$$

This holds in the SM if we neglect the CP-violating phase in the quark-mixing matrix. Even in the presence of this CP-violating phase, the CP breaking occurs at  $\mathcal{O}(\alpha^2)$  in SM W-pair production and is additionally suppressed by the smallness of the mixing angles between the quarks. Consequently in the SM one effectively has only 12 independent helicity-matrix elements instead of 36. In the presence of substantial (non-standard) CP violation this number should be increased to 18. This allows for a decomposition of the matrix elements in terms of an explicit set of 12 (18) independent basic matrix elements multiplied by purely kinematical invariant functions (coefficients) [9, 14, 15].

From the helicity amplitudes the differential cross-sections for explicit W-boson polarization and various degrees of initial-state polarization can be constructed. For example the differential cross-section for unpolarized electrons, positrons, and W bosons is given by

$$\left(\frac{d\sigma}{d\Omega}\right) = \frac{\beta}{64\pi^2 s} \sum_{\kappa, \lambda_+, \lambda_-} \frac{1}{4} |\mathcal{M}(\kappa, \lambda_+, \lambda_-, s, t)|^2. \tag{9}$$

For the numerical evaluations we have to fix the input parameters. We use the following default set [2, 26]:

$$\begin{aligned}
\alpha &\equiv \alpha(0) = 1/137.0359895, & G_{\mu} &= 1.16639 \times 10^{-5} \text{ GeV}^{-2}, \\
M_Z &= 91.1884 \text{ GeV}, & M_H &= 300 \text{ GeV}, \\
m_e &= 0.51099906 \text{ MeV}, & m_{\mu} &= 105.658389 \text{ MeV}, & m_{\tau} &= 1.7771 \text{ GeV}, \\
m_u &= 47.0 \text{ MeV}, & m_c &= 1.55 \text{ GeV}, \\
m_d &= 47.0 \text{ MeV}, & m_s &= 150 \text{ MeV}, & m_b &= 4.7 \text{ GeV}.
\end{aligned}$$

The masses of the light quarks are adjusted in such a way that the experimentally measured hadronic vacuum polarization [27] is reproduced. In the actual calculations either these light quark masses are used or the dispersion-integral result for the hadronic vacuum polarization



$M_H$ [GeV] =	60	300	1000
$M_W$ [GeV]	$m_t$ [GeV]		
80.10	119.1	137.3	154.2
80.18	133.9	151.6	168.0
80.26	148.1	165.3	181.2
80.34	161.7	178.3	193.9
80.42	174.4	190.7	206.1

Table 1: Calculated  $m_t$  for  $\alpha_s(M_Z^2) = 0.123$  and different Higgs- and W-boson masses, using the state-of-the-art calculation described in section 2.3.3. The theoretical error in  $m_t$  is roughly 1–2 GeV.

of [27]. The strong coupling constant is calculated according to the parametrization of [28], using  $\alpha_s(M_Z^2) = 0.123$  as input. The W-pair threshold region is very sensitive to  $M_W$  and consequently, if  $M_W$  were to be calculated from the other parameters using the muon decay width including radiative corrections (like at LEP1), to the masses of the top quark and Higgs boson. This is of course not very natural, since we want to use  $M_W$  as a model-independent fit parameter. In view of this we use  $\alpha$ ,  $G_\mu$ ,  $M_Z$  as input<sup>c</sup>, treat  $M_W$  as free fit parameter, and calculate  $m_t$  from muon decay<sup>d</sup>. This calculated value of  $m_t$  can then be confronted with the direct bounds from Fermilab (weighted average  $m_t = 180 \pm 12$  GeV [7]) and the indirect ones from the precision measurements at LEP1/SLC ( $m_t = 180_{-9}^{+8+17}$  GeV [2]). In this scheme  $m_t$  hence plays the role played by  $M_W$  at LEP1. The above set of parameters and the default W mass  $M_W=80.26$  GeV [2, 5] yield

$$m_t = 165.26 \text{ GeV.}$$

At present the error on this value as a result of the 160 MeV error on  $M_W$  is roughly 27 GeV. The precise  $M_W$  measurement at LEP2 will lead to a reduction of this error by a factor of four. Of course the so-obtained top-quark mass will become  $\alpha_s$ - and  $M_H$ -dependent through the RC's associated with the muon decay. We come back to that point in section 2.3.3 and only mention here that the  $M_H$  dependence of  $m_t$  amounts to roughly 33 GeV in the range  $60 \text{ GeV} < M_H < 1 \text{ TeV}$ , which clearly exceeds the above-mentioned expected error from  $M_W$  (see table 1).

Finally, the sine and cosine of the weak mixing angle are defined by

$$c_W = \cos \theta_W = \frac{M_W}{M_Z}, \quad s_W = \sin \theta_W = \sqrt{1 - c_W^2}. \quad (10)$$

---

<sup>c</sup>We do not eliminate  $M_Z$  or  $G_\mu$ , as  $M_Z$  is needed in the RC's and  $G_\mu$  reduces the size of the RC's to the production and decay of the W bosons.

<sup>d</sup>It should be noted that the RC's associated with the muon decay make that this parameter set is not overcomplete.

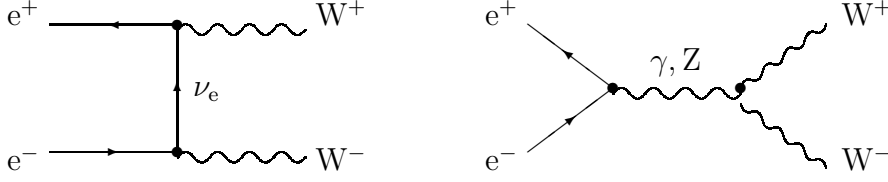


Figure 1: Lowest-order diagrams for  $e^+e^- \rightarrow W^+W^-$ .

## 2.2 Lowest order

In the SM there are three lowest-order diagrams (figure 1), if we omit a Higgs-exchange diagram that is suppressed by a factor  $m_e/M_W$  and thus completely negligible. The  $t$ -channel diagram involving the  $\nu_e$  exchange only contributes for left-handed electrons. The  $s$ -channel diagrams, containing the non-abelian triple gauge-boson couplings, contribute for both helicities of the electron. The corresponding matrix element reads

$$\mathcal{M}_{\text{Born}}(\kappa, \lambda_+, \lambda_-, s, t) = \frac{e^2}{2s_W^2} \frac{1}{t} \mathcal{M}_1^\kappa \delta_{\kappa-} + e^2 \left[ \frac{1}{s} - \frac{c_W}{s_W} g_{eeZ}^\kappa \frac{1}{s - M_Z^2} \right] 2(\mathcal{M}_3^\kappa - \mathcal{M}_2^\kappa), \quad (11)$$

with  $\delta_{\kappa-} = 1$  for left-handed electrons and  $\delta_{\kappa-} = 0$  for right-handed electrons, and

$$\mathcal{M}_1^\kappa = \bar{v}(p_+) \not{\epsilon}_+(k_+, \lambda_+) (\not{k}_+ - \not{p}_+) \not{\epsilon}_-(k_-, \lambda_-) \omega_\kappa u(p_-),$$

$$\mathcal{M}_2^\kappa = \bar{v}(p_+) \frac{\not{k}_+ - \not{k}_-}{2} [\varepsilon_+(k_+, \lambda_+) \cdot \varepsilon_-(k_-, \lambda_-)] \omega_\kappa u(p_-),$$

$$\mathcal{M}_3^\kappa = \bar{v}(p_+) (\not{\epsilon}_+(k_+, \lambda_+) [\varepsilon_-(k_-, \lambda_-) \cdot k_+] - \not{\epsilon}_-(k_-, \lambda_-) [\varepsilon_+(k_+, \lambda_+) \cdot k_-]) \omega_\kappa u(p_-). \quad (12)$$

After inserting the explicit form of the Z-boson-fermion couplings

$$g_{eeZ}^\kappa = \frac{s_W}{c_W} - \delta_{\kappa-} \frac{1}{2s_W c_W}, \quad (13)$$

we can organize the lowest-order amplitude into two gauge-invariant subsets:

$$\mathcal{M}_{\text{Born}}(\kappa, \lambda_+, \lambda_-, s, t) = \frac{e^2}{2s_W^2} \mathcal{M}_I(\kappa, \lambda_+, \lambda_-, s, t) \delta_{\kappa-} + e^2 \mathcal{M}_Q(\kappa, \lambda_+, \lambda_-, s, t), \quad (14)$$

where

$$\begin{aligned} \mathcal{M}_I(\kappa, \lambda_+, \lambda_-, s, t) &= \frac{1}{t} \mathcal{M}_1^\kappa + \frac{1}{s - M_Z^2} 2(\mathcal{M}_3^\kappa - \mathcal{M}_2^\kappa), \\ \mathcal{M}_Q(\kappa, \lambda_+, \lambda_-, s, t) &= \left[ \frac{1}{s} - \frac{1}{s - M_Z^2} \right] 2(\mathcal{M}_3^\kappa - \mathcal{M}_2^\kappa). \end{aligned} \quad (15)$$

The gauge invariance of the two contributions  $\mathcal{M}_I$  and  $\mathcal{M}_Q$  can be simply inferred from the fact that they are accompanied by different coupling constants, one of which involving the

electromagnetic coupling constant  $e$ , the other the charged-current coupling constant  $e/(\sqrt{2}s_W)$ . Whereas  $\mathcal{M}_I$  corresponds to the pure  $SU(2)$  contribution, the parity-conserving contribution  $\mathcal{M}_Q$  is a result of the symmetry-breaking mechanism.

The lowest-order cross-section determines the essential features of W-pair production. The threshold behaviour is important for the determination of the W mass from the measurement of the cross-section in a single energy point very close to threshold [8], i.e. at  $\sqrt{s} = 161$  GeV. For small  $\beta$  the matrix elements behave as

$$\mathcal{M}_2^\kappa, \mathcal{M}_3^\kappa \propto \beta, \quad \mathcal{M}_1^\kappa \propto 1 \quad (16)$$

for fixed scattering angles. Consequently, the  $s$ -channel matrix elements vanish at threshold<sup>e</sup> and the  $t$ -channel graph dominates in the threshold region. For  $\beta \ll 1$  the differential cross-section for unpolarized beams and W bosons is given by [9]

$$\left(\frac{d\sigma}{d\Omega}\right)_{\text{Born}} \approx \frac{\alpha^2}{s} \frac{1}{4s_W^4} \beta \left[1 + 4\beta \cos\theta \frac{3c_W^2 - 1}{4c_W^2 - 1} + \mathcal{O}(\beta^2)\right], \quad (17)$$

where the leading term  $\propto \beta$  originates from the  $t$ -channel diagram only. Note that the leading term is angular-independent. In the total cross-section

$$\sigma_{\text{Born}} \approx \frac{\pi\alpha^2}{s} \frac{1}{4s_W^4} 4\beta + \mathcal{O}(\beta^3), \quad (18)$$

all terms  $\propto \beta^2$  drop out and the  $s$ -channel and the  $s$ - $t$ -interference contributions are proportional to  $\beta^3$ . This is the consequence of CP conservation, fermion-helicity conservation in the initial state, and the orthogonality of different partial waves [9]. Hence in the threshold region the  $t$  channel is dominant and the cross-section for  $e^+e^- \rightarrow W^+W^-$  is not very sensitive to the triple gauge-boson couplings.

In table 2 we give the integrated cross-section for different centre-of-mass energies and different polarizations of the electrons (+, -). Positrons are assumed to be unpolarized. Using right-handed electrons one could study a pure triple-gauge-coupling process, but this would require longitudinally polarized electron beams, the prospect of which looks rather unfavourable for LEP2. Furthermore, for all energies the cross-section for right-handed electrons is suppressed by two orders of magnitude compared with the dominant left-handed mode, mainly because there is no  $t$ -channel contribution. Therefore essentially only the latter can be investigated at LEP2. With transverse beam polarization, however, one could obtain information on the right-handed matrix element via its interference with the left-handed one.

As stated in section 2.1, for on-shell W-pair production and unpolarized electrons and positrons there are nine independent helicity-matrix elements or six if CP is conserved. These yield nine or six independent observables. Taking into account the decay of the W bosons there are many more observables: 81 or, if CP is conserved, 36 products of the various helicity-matrix

---

<sup>e</sup>This holds for arbitrary CP-conserving  $s$ -channel contributions in the limit of vanishing electron mass [11].

$\sqrt{s}$ [GeV]	$\sigma_{\text{Born}}$	$\sigma_{\text{Born}}^-$	$\sigma_{\text{Born}}^+$
161.0	3.812	7.622	0.002
175.0	15.959	31.716	0.202
184.0	17.427	34.567	0.287
190.0	17.762	35.203	0.321
205.0	17.609	34.867	0.350

Table 2: Integrated lowest-order cross-section in pb for different polarizations of the electrons and different centre-of-mass energies.

elements [11]. Because the  $V - A$  structure of the W decays is well established, these observables can be extracted in a model-independent way from the data for the five-fold differential cross-section  $d\sigma/(d\cos\theta d\cos\theta_1 d\phi_1 d\cos\theta_2 d\phi_2)$ , where  $\theta_{1,2}$  and  $\phi_{1,2}$  represent the decay angles of the two W bosons. These observables may serve to put limits on anomalous couplings [10, 12]. Note that the five-fold differential cross-section requires the identification of the charge of at least one of the decaying W bosons, as otherwise the information on the sign of  $\cos\theta$  would be lost. This is possible for hadronic–leptonic or leptonic–leptonic events. If no charge identification is possible only production–forward–backward–symmetric observables would be left. As argued above, in those observables for instance the  $s$ -channel contribution is suppressed by  $\beta^2$  in the threshold region<sup>f</sup>. Consequently, if one cannot identify the jet charges the purely hadronic events will not be of much use for studies of the gauge couplings at LEP2. Of course this does not concern the W-mass determination as it does not rely on  $s$ -channel contributions.

## 2.3 Radiative corrections

As has been argued in section 1, the SM theoretical predictions for W-pair production should have an uncertainty of about 0.5% (2% at  $\sqrt{s} = 161$  GeV) in order to obtain reasonable limits on the structure of the gauge-boson self-couplings, and to determine the W-boson mass with the envisaged precision of roughly 40–50 MeV. In this context radiative corrections are indispensable.

Much effort has been made in recent years to obtain such precise theoretical predictions for W-pair production. In the following we discuss the existing results for the virtual and real electroweak corrections in the on-shell case. In addition we discuss the quality of an improved Born approximation (IBA) that contains all familiar, LEP1-like leading corrections for the W-pair production cross-section at LEP2 energies. Such a discussion is in particular relevant as the present off-shell LEP2 Monte Carlos often make use of such an approximation.

---

<sup>f</sup>If CP is violated there exists an anomalous gauge-boson coupling that does not yield a suppressed  $s$ -channel contribution [9, 11].

### 2.3.1 Radiative electroweak $\mathcal{O}(\alpha)$ corrections

The  $\mathcal{O}(\alpha)$  radiative corrections can be naturally divided into three classes, the virtual, soft-photon, and hard-photon contributions. Since the process  $e^+e^- \rightarrow W^+W^-$  involves the charged current in lowest order, the corresponding radiative corrections cannot be separated on the basis of Feynman diagrams into electromagnetic and weak contributions in a gauge-invariant way. Like we have already observed in equation (15),  $SU(2)$  gauge invariance requires an interplay between the  $\gamma$ - and  $Z$ -exchange diagrams.

The complete radiative electroweak  $\mathcal{O}(\alpha)$  corrections have been calculated independently by two groups [14, 15]<sup>9</sup>. For the unpolarized case they have been checked and found to agree within a couple of per-mil (i.e. within the integration error).

The virtual corrections contain infra-red (IR) divergences, which result from virtual photons exchanged between external charged particles. They are compensated for by adding the cross-section for the process  $e^+e^- \rightarrow W^+W^-\gamma$ . If the energy of the emitted photon is small compared with the detector resolution (soft photons), this process cannot be distinguished experimentally from the non-radiative  $W$ -pair production process. In practical experiments the soft-photon approximation is in general not sufficient and one has to include the radiation of hard photons, too. When adding these real-photon effects to the contribution of the virtual corrections, not only the IR singularities but also the large Sudakov double logarithms  $\log^2(s/m_e^2)$  drop out.

Still there are various sources of potentially large  $\mathcal{O}(\alpha)$  corrections left at LEP2 energies. First of all there are large QED corrections of the form  $(\alpha/\pi) \log(Q^2/m_e^2)$  with  $Q^2 \gg m_e^2$ , originating from collinear photon radiation off the electron or positron (see appendix A). They form a gauge-invariant subset of QED corrections and amount to roughly 6% at LEP2, not taking into account possible enhancements from the corresponding coefficients (like, e.g., close to thresholds).

From the renormalization two sets of potentially large fermionic (formally weak) corrections arise. The first set is associated with the charge renormalization at zero momentum transfer, where the relevant scale is set by the fermion masses entering the vacuum polarization. In high-energy experiments, however, the running charge should be evaluated at scales much larger than the masses of the light fermions  $f_\ell = \{e, \mu, \tau, u, d, c, s, b\}$ . This leads to large logarithmic ('mass singular') contributions of the form  $(\alpha/\pi) \log(Q^2/m_{f_\ell}^2)$  with  $Q^2 \gg m_{f_\ell}^2$ , which can amount to a shift in  $\alpha$  of 8% at LEP2 energies. Related to the top quark, corrections  $\propto m_t^2/M_W^2$  will occur. They show up as universal corrections via the renormalization of the  $W$  and  $Z$  masses (or equivalently  $s_W^2$ ) if the corresponding renormalization scales are small compared with the mass splitting in the  $(t, b)$  isospin doublet.

Finally the long-range electromagnetic interaction between the slowly moving  $W$  bosons leads to the so-called Coulomb singularity [30]. This singularity yields an  $\mathcal{O}(\alpha)$  correction factor  $\alpha\pi/(2\beta)$ , resulting in an  $\mathcal{O}(\alpha)$ -corrected cross-section that does not vanish at threshold for left-

---

<sup>9</sup>The process  $e^+e^- \rightarrow W^+W^-\gamma$  has also been calculated in [29].

$M_H$ [GeV] =	300	300	300	60	300	1000
$\alpha_s$ =	0.117	0.123	0.129	0.123	0.123	0.123
$m_t$ [GeV] =	164.80	165.26	165.73	148.14	165.26	181.20
$\sqrt{s}$ [GeV]	$\sigma$ [pb]					
161.0	2.473	2.472	2.470	2.514	2.472	2.460
175.0	14.471	14.465	14.459	14.548	14.465	14.422
184.0	16.619	16.613	16.607	16.671	16.613	16.568
190.0	17.263	17.257	17.251	17.301	17.257	17.213
205.0	17.683	17.677	17.671	17.698	17.677	17.637

Table 3: Integrated unpolarized cross-section including radiative electroweak  $\mathcal{O}(\alpha)$  corrections for different values for the Higgs-boson mass and  $\alpha_s$ , at various centre-of-mass energies. The theoretical error in  $m_t$  is roughly 1–2 GeV.

handed electrons. The right-handed cross-section remains suppressed by at least  $\beta^2$ . This correction factor exhibits the fact that the free-particle approximation is inadequate near the W-pair production threshold in the presence of the long-range Coulomb interaction. We want to stress here that the Coulomb singularity is changed substantially by effects that effectively truncate the range of the interaction, like the off-shellness and the decay of the W bosons. This will be treated in section 3.4.2 and will lead to the conclusion that higher-order Coulombic corrections to the total cross-section are not important.

The sensitivity of the total unpolarized cross-section to  $\alpha_s$  and the unknown mass of the Higgs boson is illustrated in table 3. The dependence on  $\alpha_s$ , originating from the calculation of  $m_t$ , is completely negligible ( $\lesssim 0.1\%$ ). Compared with the lowest-order cross-sections of table 2, a variation of  $M_H$  between 60 and 1000 GeV, however, influences the total cross-section by around 0.5% at the three highest energy points, by about 0.8% at  $\sqrt{s} = 175$  GeV, and by 1.4% at threshold. These numbers are lowered by about 0.5% if the radiative corrections are calculated in the so-called  $G_\mu$  representation, which absorbs the universal  $m_t$  and  $M_H$  effects present in the W wave-function factors (see section 2.4.2). In this representation a variation of  $M_H$  between 300 and 1000 GeV has a negligible impact on the cross-section. Keeping in mind that we would like to reach a theoretical accuracy of 2% (0.5%) at  $\sqrt{s} = 161$  GeV ( $\sqrt{s} \geq 175$  GeV), it should be clear that the Higgs-mass dependence constitutes a major uncertainty. A more detailed investigation [31] revealed that this Higgs-boson-mass dependence is the result of the Yukawa interaction between the two slowly moving W bosons (mediated by the Higgs boson). As such the effect is largest close to threshold and for the lightest Higgs masses, which

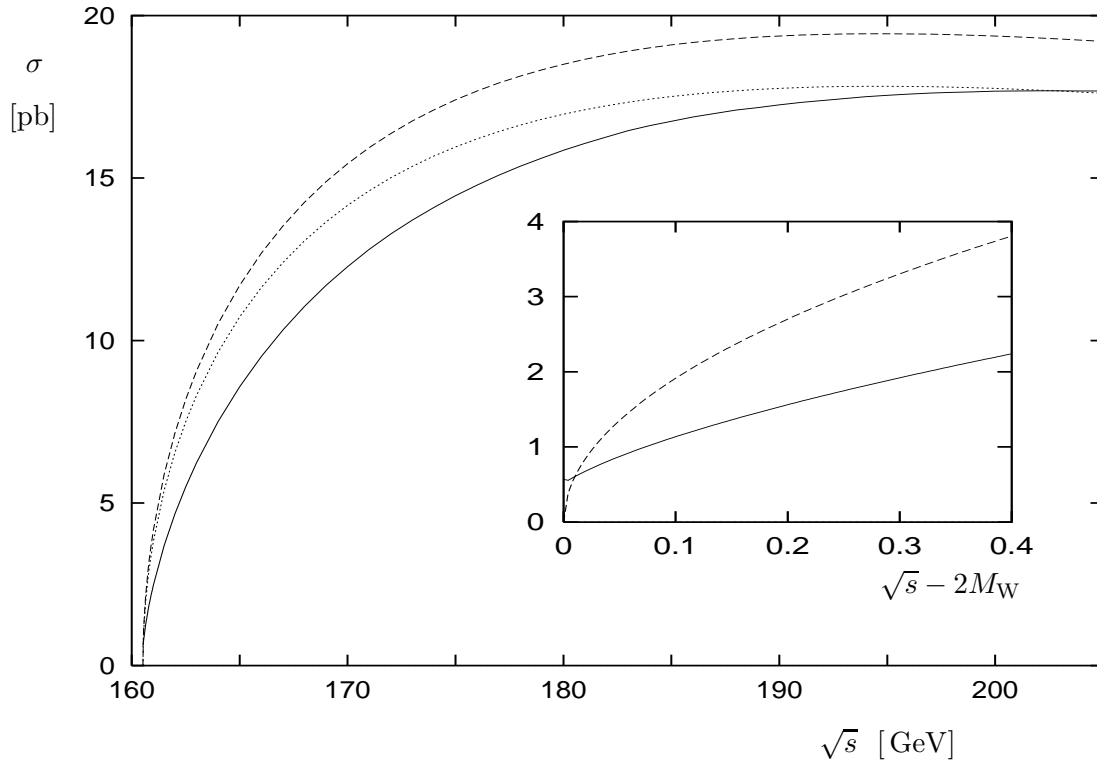


Figure 2: Unpolarized total cross-section in the threshold region. The dotted curve corresponds to Born, the dashed one to  $G_\mu$ -Born, and the solid one to the results including full radiative electroweak  $\mathcal{O}(\alpha)$  corrections.

yield the shortest range of the interaction. For instance, upon increasing the lower Higgs-mass bound from 60 to 90 GeV, the resulting uncertainty is reduced by roughly a factor of two<sup>*h*</sup>.

In figure 2 we display the influence of the full  $\mathcal{O}(\alpha)$  corrections on the total unpolarized cross-section near the W-pair production threshold.

As has been stated before, it should be noted that, unlike at LEP1, the presence of the charged current at lowest order in  $e^+e^- \rightarrow W^+W^-$  complicates the separation between QED and weak corrections. So, in order to have a cleaner look at the QED corrections we present in addition to the Born cross-section also the lowest-order cross-section in the so-called  $G_\mu$  representation, i.e. the Born cross-section with  $\alpha$  replaced by  $\sqrt{2} G_\mu M_W^2 s_W^2 / \pi$ , which already contains an important part of the leading weak effects discussed above<sup>*i*</sup> (see also section 2.3.3). We will refer to this cross-section as  $G_\mu$ -Born. As a result of the steep drop with decreasing centre-of-mass energy of the W-pair cross-section close to threshold, large and predominantly

<sup>*h*</sup>At the start of the 161 GeV run no significant change in the  $M_H$  bound is expected. So, only after the higher-energy LEP2 runs have taken place the improved knowledge on  $M_H$  can be used for an a posteriori reduction of the  $M_H$  dependence of the 161 GeV run.

<sup>*i*</sup>As the  $t$  channel is dominant at LEP2 energies, the  $G_\mu$ -Born describes the leading weak corrections reasonably well for the default Higgs mass  $M_H=300$  GeV.

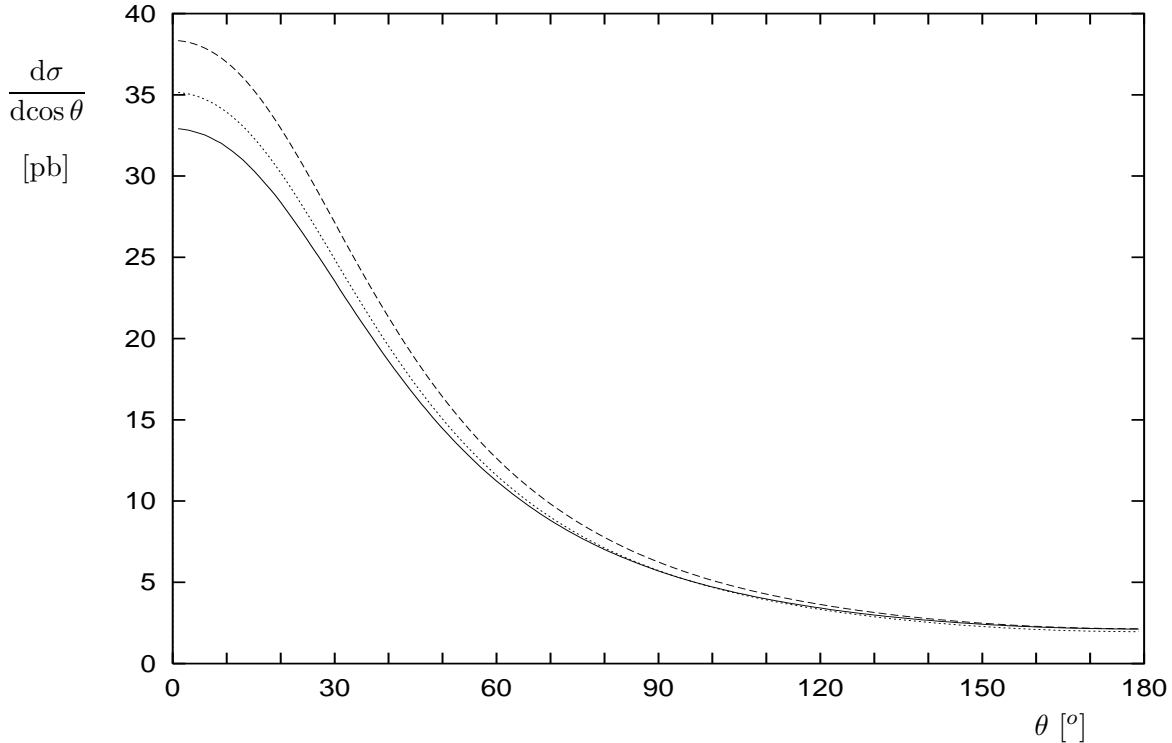


Figure 3: Unpolarized differential cross-section  $d\sigma/(d\cos\theta_+)$  at  $\sqrt{s} = 190$  GeV. The same signature as adopted in figure 2.

soft QED effects can be observed. Compared with  $G_\mu$ -Born the  $\mathcal{O}(\alpha)$  corrections amount to more than  $-25\%$  in the direct vicinity of the threshold ( $\sqrt{s} < 165$  GeV), apart from the region very close to threshold where the positive Coulomb-singularity contribution takes over (see close-up in figure 2), and still  $-17\%$  ( $-11\%$ ) at  $\sqrt{s} = 175$  GeV (190 GeV). The size of these effects necessitates the inclusion of higher-order QED corrections in order to end up with an acceptable theoretical uncertainty. A discussion of these higher-order QED corrections can be found in section 2.3.3. The finite W width has a drastic impact on the effects related to the Coulomb singularity (see section 3.4.2), but the large soft QED effects are merely smoothed and stay sizeable.

In figure 3 the effect of the  $\mathcal{O}(\alpha)$  corrections on the unpolarized differential cross-section  $d\sigma/(d\cos\theta_+)$  is shown for  $\sqrt{s} = 190$  GeV. Here  $\theta_+$  stands for the polar angle of the  $W^+$  boson with respect to the incoming positron<sup>*j*</sup>. Apart from the expected normalization effects that are already observed in the total cross-section, also a distortion of the distribution occurs. As this is exactly the type of signature one might expect from anomalous gauge-boson couplings, this underlines again the importance of having a profound knowledge of the SM radiative corrections. The origin of the distortion can be traced back to hard initial-state photonic corrections. Hard-photon emissions boost the centre-of-mass system of the  $W^+W^-$  pair. As a

<sup>*j*</sup>In the presence of hard-photon radiation in general  $\theta_+ \neq \theta_-$ .



result of that, events that are forward in the centre-of-mass system of the produced W bosons can show up as backward events in the LAB system and vice versa. Since the cross-section in the backward direction is substantially lower than in the forward direction, the net effect of this redistribution (migration) of events will be a distortion of the differential distribution with respect to the lowest-order one. Of course these boost effects are much more pronounced at high energies [9].

### 2.3.2 Approximations in the LEP2 region

The complete analytic results for the electroweak  $\mathcal{O}(\alpha)$  corrections are very lengthy and complicated, resulting in huge and rather slow computer programs. Moreover, the formulae are completely untransparent. In view of this, simple approximative expressions are desirable. Apart from providing fast computer programs, which are useful for many applications, simple transparent formulae should reveal the physical content and the origin of the dominant radiative corrections. Furthermore, if these approximative expressions represent the exact corrections adequately, one might consider implementing them in the existing LEP2 Monte Carlos.

Owing to the lack of a calculation of the complete  $\mathcal{O}(\alpha)$  corrections, the present LEP2 Monte Carlos for off-shell W-pair production include only the known leading universal corrections. In order to assess the theoretical uncertainty inherent in this approach, the on-shell case can be used as guideline. The size of the non-leading  $\mathcal{O}(\alpha)$  corrections in this case should provide a reasonable estimate for the corresponding left-out non-leading corrections in the off-shell case.

We start out by investigating the structure of the matrix element for  $e^+e^- \rightarrow W^+W^-$ . Whereas it involves only three different tensor structures in lowest order, at  $\mathcal{O}(\alpha)$  twelve independent tensor structures occur, each of which is associated with an independent invariant function, which can be considered as an  $s$ - and  $t$ -dependent effective coupling. The dominant radiative corrections, as e.g. those that are related to UV, IR, or mass singularities, in general have factorization properties and are at  $\mathcal{O}(\alpha)$  restricted to those invariant functions that appear already at lowest order. Therefore the contributions of the other invariant functions should be relatively small. Indeed, a numerical analysis reveals that in a suitably chosen representation for the basic set of independent matrix elements only the three Born-like invariant functions plus one extra right-handed piece, related to  $\mathcal{M}_I^+$ , are relevant for a sufficiently good approximation [32, 33]. This results in the following approximation for the matrix element:

$$\mathcal{M}_{\text{app}}^\kappa = \mathcal{M}_I^\kappa F_I^\kappa + \mathcal{M}_Q^\kappa F_Q^\kappa, \quad (19)$$

with  $\mathcal{M}_I$  and  $\mathcal{M}_Q$  defined in equation (15). The term involving  $F_I^+$  is needed for right-handed electrons because of contributions  $\propto \beta^2 \cos \theta$ , originating from the interference of  $\mathcal{M}_{\text{Born}}$  with particular 1-loop matrix elements, which are not present at lowest order. Neglecting the other invariant functions in the basis given in [32] introduces errors well below the per-cent level (see table 4). This is of course only true for observables where  $\mathcal{M}_{\text{app}}^\kappa$  is not suppressed or absent. All this demonstrates that improved Born approximations are possible. Note, however,

that in contrast to the situation at LEP1 the invariant functions  $F_{I,Q}^\kappa$  are both energy- and angular-dependent.

In order to construct an improved Born approximation (IBA) one has to specify simple expressions for the invariant functions  $F_{I,Q}^\kappa$ , which reproduce the corresponding exact expressions with sufficient accuracy. In the LEP2 energy region the following expressions can be used as a reasonable ansatz [32]

$$\begin{aligned} F_I^\kappa &= \left[ 2\sqrt{2} G_\mu M_W^2 + \frac{4\pi\alpha}{2s_W^2} \frac{\pi\alpha}{4\beta} (1 - \beta^2)^2 \right] \delta_{\kappa-}, \\ F_Q^\kappa &= \left[ 4\pi\alpha(s) + 4\pi\alpha \frac{\pi\alpha}{4\beta} (1 - \beta^2)^2 \right]. \end{aligned} \quad (20)$$

The terms containing  $G_\mu$  and  $\alpha(s)$  incorporate all the leading universal corrections associated with the running of  $\alpha$  and the corrections  $\propto \alpha m_t^2/M_W^2$  associated with the  $\rho$  parameter (see also section 2.3.3). As these are linked to the renormalization of the electric charge at zero momentum transfer and of the weak mixing angle, they only contribute to the structures already present at lowest order. The corresponding leading  $\mathcal{O}(\alpha)$  contributions can be recovered from equation (20) by substituting

$$\alpha(s) \rightarrow \alpha[1 + \Delta\alpha(s)], \quad 2\sqrt{2} G_\mu M_W^2 \rightarrow \frac{4\pi\alpha}{2s_W^2} \left[ 1 + \Delta\alpha(M_W^2) - \frac{c_W^2}{s_W^2} \Delta\rho \right], \quad (21)$$

with

$$\Delta\alpha(s) = \frac{\alpha}{3\pi} \sum_{f \neq t} N_C^f Q_f^2 \log\left(\frac{s}{m_f^2}\right), \quad \Delta\rho = \frac{3\alpha m_t^2}{16\pi s_W^2 M_W^2}. \quad (22)$$

The  $1/\beta$  term describes the effect of the Coulomb singularity, which for  $\beta \ll 1$  yields a simple correction factor to the lowest-order cross-section:

$$\delta\sigma_{\text{Coul}} = \frac{\pi\alpha}{2\beta} \sigma_{\text{Born}}. \quad (23)$$

The factor  $(1 - \beta^2)^2$  is introduced by hand to switch off the Coulomb singularity fast enough. In this way one avoids corrections that are too large away from threshold, where the Coulomb singularity should not play a role anymore. As has been studied in [32], heavy-mass contributions  $\propto \log(m_t)$  and  $\log(M_H)$  that are not covered by equation (20) have a negligible impact on the approximation. Since the above IBA analysis has been performed for the default Higgs-boson mass  $M_H = 300$  GeV, the large light-Higgs-boson corrections close to threshold, shown in table 3, are absent. By adding a simple approximation for these corrections [31] to the IBA, however, the full  $M_H$  dependence of the exact  $\mathcal{O}(\alpha)$  corrections can be reproduced.

In addition to the contributions described so far, one has to include the leading logarithmic QED corrections. These can be calculated using the structure-function method as described in appendix A. They comprise all contributions  $\propto (\alpha/\pi) \log(m_e^2/Q^2)$ . In the following numerical

analysis the scale  $Q^2 = s$  has been used and, in order to extract the effect of the non-leading virtual corrections, hard-photon radiation is left out.

As we want to compare the approximation with an  $\mathcal{O}(\alpha)$  calculation we do not use the square of the matrix element defined in equations (19) and (20) for the numerical analysis, but only the square of the terms involving  $G_\mu$  and  $\alpha(s)$  and the interference of these terms with the others. Moreover, in this interference  $G_\mu$  and  $\alpha(s)$  are replaced by the corresponding lowest-order expressions in terms of  $s_W^2$  and  $\alpha(0)$ . Nevertheless, the so-obtained approximation still contains higher-order contributions through the squares of  $\alpha(s)$  and  $G_\mu$ . To allow for a meaningful comparison these have been included in the numbers for the exact one-loop results given in table 4 in the same way (see [32] for more details).

In table 4 we show the difference between the exact and approximated virtual and soft  $\mathcal{O}(\alpha)$  radiative corrections to the total and differential cross-section for right-handed, left-handed, and unpolarized electrons. The positrons are assumed to be unpolarized. In the LEP2 energy region the relative difference between the exact result and the approximation can be as large as 1–2% for left-handed or unpolarized electrons, and reach 3–8% for right-handed electrons. As there is no obvious reason why these remaining non-leading corrections should be smaller in the case of off-shell W bosons or  $e^+e^- \rightarrow 4f$ , their inclusion in the LEP2 data analysis seems to be unavoidable.

### 2.3.3 Higher-order corrections

In section 2.3.1 we have encountered large  $\mathcal{O}(\alpha)$  corrections. A short description of the way to include the corresponding higher-order corrections is hence in place.

In two distinct ways the higher-order corrections enter the calculation of the distributions for W-pair production. First of all there is the calculation of  $m_t$  from  $M_W$  and the input parameters, either to be used in the calculation of the W-pair RC's or to be confronted with the Tevatron data. As  $m_t$  enters the relation between  $\alpha$ ,  $G_\mu$ ,  $M_Z$ , and  $M_W$ , resulting from the muon decay width, at the 1-loop level, the highest precision possible is required for this relation. As this relation relies on calculations performed at  $Q^2 \approx 0$  for the muon decay width and at the subtraction points  $Q^2 = M_W^2, M_Z^2$  for the renormalization procedure, we can use the state-of-the-art calculation developed for the LEP1 analysis [6]. This yields

$$G_\mu = \frac{\alpha\pi}{\sqrt{2}s_W^2 M_W^2} \rho_c. \quad (24)$$

Usually  $\rho_c$  is written in the form

$$\rho_c = \frac{1}{1 - \Delta r}, \quad (25)$$

	unpolarized		right-handed		left-handed	
$\sqrt{s} = 161 \text{ GeV}$						
total	1.45	0.00	-1.56	-0.01	1.45	0.00
10°	1.63	0.00	4.41	0.00	1.63	0.00
90°	1.44	0.00	-1.57	-0.01	1.44	0.00
170°	1.26	0.00	-7.52	0.00	1.26	0.00
$\sqrt{s} = 165 \text{ GeV}$						
total	1.27	0.02	-2.09	-0.01	1.28	0.02
10°	1.67	0.00	0.49	0.00	1.67	0.00
90°	1.17	0.02	-2.09	-0.02	1.18	0.02
170°	0.75	0.00	-4.64	0.00	0.77	0.00
$\sqrt{s} = 175 \text{ GeV}$						
total	1.26	0.03	-2.58	-0.02	1.28	0.03
10°	1.71	0.00	0.18	0.00	1.71	0.00
90°	1.03	0.05	-2.59	-0.03	1.06	0.05
170°	0.59	0.00	-5.30	0.00	0.69	0.00
$\sqrt{s} = 184 \text{ GeV}$						
total	1.02	0.04	-2.80	-0.03	1.06	0.04
10°	1.57	0.00	2.17	-0.01	1.57	0.00
90°	0.67	0.08	-2.82	-0.05	0.72	0.08
170°	0.10	0.00	-7.72	0.01	0.32	0.00
$\sqrt{s} = 190 \text{ GeV}$						
total	1.24	0.03	-2.91	-0.04	1.28	0.03
10°	1.67	0.00	0.59	-0.01	1.67	0.00
90°	0.95	0.06	-2.92	-0.06	1.01	0.06
170°	0.58	0.00	-6.32	0.00	0.83	0.00
$\sqrt{s} = 205 \text{ GeV}$						
total	1.60	0.00	-3.11	-0.09	1.65	0.00
10°	1.77	0.00	-1.68	-0.01	1.77	0.00
90°	1.55	0.00	-3.14	-0.12	1.64	0.00
170°	1.61	0.00	-4.37	0.00	1.94	0.00

Table 4: Quality of the IBA (first column per polarization) and the form-factor approximation (19) (second column per polarization), given in per cent relative to Born. Results are given for the total cross-section (total) and the differential cross-section at 10, 90, and 170°.

where  $\Delta r$  contains all the one-loop corrections to the muon decay width with the inclusion and the proper arrangement of the higher-order terms. Next we subdivide  $\rho_c$  as introduced in equation (25) into a *leading* term,  $\Delta r_L$ , and *remainder* terms,  $\Delta r_{\text{rem}}$ , as follows:

$$\rho_c = \frac{1}{1 - \Delta r} = \frac{1}{1 - \Delta r_L - \Delta r_{\text{rem}}} = \frac{1}{(1 - \Delta\alpha) \left(1 + \frac{c_W^2}{s_W^2} \Delta\rho_X\right) - \Delta r_{\text{rem}}}, \quad (26)$$

with

$$\Delta r_{\text{rem}} = \Delta r^\alpha + \Delta r^{\alpha\alpha_s} + \frac{c_W^2}{s_W^2} \Delta\bar{\rho}_X - \Delta\alpha. \quad (27)$$

This contains all the terms known at present: the complete one-loop  $\mathcal{O}(\alpha)$  corrections  $\Delta r^\alpha$  (two-, three-, four-point functions) and complete two-loop  $\mathcal{O}(\alpha\alpha_s)$  insertions  $\Delta r^{\alpha\alpha_s}$  to two-point functions, from which the leading  $\mathcal{O}(\alpha)$  and  $\mathcal{O}(\alpha\alpha_s)$  terms are subtracted. The Born version of equation (24), i.e.  $\rho_c = 1$ , relates  $G_\mu$  directly to  $\alpha$ ,  $M_W$ , and  $M_Z$ , hence leaving no room for using  $G_\mu$  as additional independent input parameter. However, having introduced radiative corrections to the Born relation we can solve equation (24) in terms of the top quark mass and, in turn, this particular value for  $m_t$  will be used throughout the rest of the calculation. One should notice that this procedure is not free of ambiguities since  $\Delta r$  is also a function of  $M_H$ , but with much smaller sensitivity due to the well known screening. So in the end we should also allow for some variation in  $M_H$ . Moreover,  $\Delta r$  is also a function of  $\alpha_s$  through higher-order corrections, for instance  $\mathcal{O}(\alpha\alpha_s)$ , and, as a consequence, also some variation in the strong coupling constant should be allowed.

The leading terms  $\Delta\alpha$  and  $\Delta\bar{\rho}_X$  appearing in equation (27) are given by

$$\begin{aligned} \Delta\bar{\rho}_X &= \Delta\bar{\rho}^\alpha + \Delta\bar{\rho}^{\alpha\alpha_s} + \bar{X} \\ &= \frac{3\alpha}{16\pi s_W^2 c_W^2} \frac{m_t^2}{M_Z^2} \left[ 1 - \frac{2}{3} \left( 1 + \frac{\pi^2}{3} \right) \frac{\alpha_s(m_t^2)}{\pi} \right] + \bar{X}, \\ \Delta\alpha &= 1 - \frac{\alpha}{\alpha(M_W^2)}, \\ \alpha(s) &= \frac{\alpha}{1 + \Sigma_\gamma^{f \neq t}(s)/s}, \end{aligned} \quad (28)$$

where  $\Sigma_\gamma^{f \neq t}(s)$  is the renormalized  $\mathcal{O}(\alpha)$  transverse photon self-energy originating from fermion loops, excluding top-quark loops.

The term  $\bar{X}$  in equation (28) is a next-to-leading order term, whose proper treatment is rather important:

$$\bar{X} = \text{Re} \left[ \frac{\Pi_Z(M_Z^2)}{M_Z^2} - \frac{\Pi_W(M_W^2)}{M_W^2} \right]_{\overline{\text{MS}}}^{\text{1loop}} - \Delta\rho^\alpha, \quad (29)$$

where  $\Pi_V$  denotes the unrenormalized transverse self-energy of the  $V$  gauge boson. The ultraviolet (UV) divergences are removed according to the  $\overline{\text{MS}}$  renormalization scheme with  $\mu = M_Z$ .

In contrast to  $\Delta\bar{\rho}_X$ , the leading contribution  $\Delta\rho_X$  appearing in equation (26) is normalized by  $G_\mu$  rather than by  $\alpha/(s_W^2 M_W^2)$ , as is required by the resummation proposed in [34]:

$$\begin{aligned}\Delta\rho_X &= \Delta\rho^\alpha + \Delta\rho^{\alpha^2} + \Delta\rho^{\alpha\alpha_s} + \Delta\rho^{\alpha\alpha_s^2} + X \\ &= N_C^t x_t \left[ 1 + x_t \Delta\rho^{(2)} \left( \frac{m_t^2}{M_H^2} \right) + c_1 \frac{\alpha_s(m_t^2)}{\pi} + c_2 \left( \frac{\alpha_s(m_t^2)}{\pi} \right)^2 \right] + X,\end{aligned}\quad (30)$$

where  $N_C^t = 3$  and

$$x_t = \frac{G_\mu}{\sqrt{2}} \frac{m_t^2}{8\pi^2}, \quad (31)$$

$$X = 2s_W^2 c_W^2 \frac{G_\mu M_Z^2}{\sqrt{2}\pi\alpha} \bar{X}. \quad (32)$$

The coefficients  $c_1$  and  $c_2$  describe the first- and second-order QCD corrections for the leading  $x_t$  contribution to  $\Delta\rho$ , calculated in [35, 36]. Correspondingly:

$$c_1 = -\frac{2}{3} \left( 1 + \frac{\pi^2}{3} \right), \quad (33)$$

$$c_2 = -\pi^2 (2.564571 - 0.180981 n_f), \quad (34)$$

with  $n_f$  the total number of flavours ( $n_f = 6$ ). The function  $\Delta\rho^{(2)}(m_t^2/M_H^2)$  describes the leading two-loop electroweak  $x_t$  correction to  $\Delta\rho$ , calculated first in the  $M_H = 0$  approximation in [37] and later in [38] for an arbitrary relation between  $M_H$  and  $m_t$ .

It should be noted that the higher-order radiative corrections discussed above are usually calculated in the limit of a heavy top mass, i.e. usually only the leading part of the corrections is under control. This often raises the question of what effect can be estimated from the sub-leading terms, since  $m_t \approx 2M_Z$ . As far as QCD  $\mathcal{O}(\alpha_s)$  and  $\mathcal{O}(\alpha_s^2)$  corrections are concerned the sub-leading terms are well under control. In the pure electroweak sector, however, there has been, so far, no calculation of higher-order sub-leading terms at an arbitrary scale. The only available piece of calculation concerns the  $\rho$  parameter at  $Q^2 = 0$  [39], therefore relevant only for  $\nu_\mu e$  scattering. If however one is willing to extrapolate the  $Q^2 = 0$  result to a higher scale, by assuming that the ratio of leading to next-to-leading corrections is representative for the corresponding theoretical uncertainty, then the answer is next-to-leading  $\approx$  leading.

Even before considering the actual impact of the higher-order terms on  $m_t$ , we should mention at this point that the way in which the non-leading terms can be treated and the exact form of the *leading-remainder* splitting give rise to several possible options in the actual implementation of radiative corrections. This in turn becomes a source of theoretical uncertainty. For instance, for  $\Delta r$  we can introduce the decomposition into leading and remainder. Since we know how to proceed with all objects in the leading approximation, the only ambiguity is due to the treatment of the remainders. Clearly, after the splitting  $\Delta r = \Delta r_L + \Delta r_{\text{rem}}$  there are in principle several possible ways of handling the remainder:

$$\frac{1}{1 - \Delta r} = \frac{1}{1 - \Delta r_L - \Delta r_{\text{rem}}}, \quad \frac{1}{1 - \Delta r_L} \left( 1 + \frac{\Delta r_{\text{rem}}}{1 - \Delta r_L} \right), \quad \frac{1 + \Delta r_{\text{rem}}}{1 - \Delta r_L}, \quad \frac{1}{1 - \Delta r_L} + \Delta r_{\text{rem}}. \quad (35)$$

Actually, these options differ among themselves, but the difference can be related to the choice of the scale in the remainder term. A complete evaluation of the sub-leading  $\mathcal{O}(G_\mu^2 M_Z^2 m_t^2)$  corrections would greatly reduce the associated uncertainty. In conclusion, we observe that a natural and familiar language for the basic ingredients of the physical observables is that of effective couplings. However, it should be stressed that the above formulae belong to a specific realization of this language and other realizations could also be used.

Now we can assess the influence of the higher-order corrections on the calculation of  $m_t$  from equation (24). Using for instance  $M_W = 80.26$  GeV and  $M_Z = 91.1884$  GeV we find

$$m_t = 165_{-18}^{+16}(M_H, \alpha_s) \text{ GeV}, \quad (36)$$

the central value of which corresponds to  $M_H = 300$  GeV and  $\alpha_s(M_Z^2) = 0.123$ . The errors are derived by varying  $M_H$  and  $\alpha_s$  in the range  $60 \text{ GeV} < M_H < 1 \text{ TeV}$  and  $\alpha_s = 0.123 \pm 0.006$ . It should be noted in this respect that the total variation induced by  $M_H$  alone (at  $\alpha_s = 0.123$ ) is about 33 GeV. The following is observed for the higher-order corrections:

- by neglecting the  $\mathcal{O}(\alpha^2)$  term in  $\Delta r$  we find for the same input parameters (and  $M_H = 300$  GeV,  $\alpha_s = 0.123$ ) a shift in  $m_t$  of  $-1.9$  GeV.
- If instead we switch off the  $\mathcal{O}(\alpha\alpha_s^2)$  correction the corresponding shift will be  $-1.5$  GeV.
- If finally both the  $\mathcal{O}(\alpha\alpha_s)$  and  $\mathcal{O}(\alpha\alpha_s^2)$  corrections are neglected we find a shift in  $m_t$  of  $-10.5$  GeV. Here by  $\mathcal{O}(\alpha\alpha_s)$  the full result is implied and not only the leading part of it.

Based on the above observations, the remaining theoretical uncertainty in the calculation of  $m_t$  from missing higher-order corrections and sub-leading  $\mathcal{O}(\alpha^2)$  corrections to  $\Delta r$  is estimated to be roughly 1–2 GeV.

The second way the higher-order corrections enter the calculations for W-pair production is through the process itself, so through self-energies, vertices, etc. The known weak higher-order effects comprise the running of  $\alpha$  [see equation (28)] and the complete  $\mathcal{O}(\alpha\alpha_s)$  corrections to the gauge-boson self-energies [35]. Other higher-order calculations, as those for  $\Delta\rho$  at  $\mathcal{O}(\alpha^2)$  or  $\mathcal{O}(\alpha\alpha_s^2)$ , have been performed in the limit where  $m_t$  is the largest scale. The QCD corrections associated with the gauge-boson vertex corrections have, to our knowledge, not been calculated yet, but they are at most logarithmic in the top mass. If one takes into account the leading weak effects by replacing  $e^2/(2s_W^2)$  by  $2\sqrt{2}G_\mu M_W^2$  in the  $\mathcal{M}_I$  part of equation (15) and  $\alpha$  by  $\alpha(s)$  in the  $\mathcal{M}_Q$  part, the remaining unknown higher-order weak effects are expected to be negligible compared with the required theoretical accuracy.

As pointed out in the previous subsection, the virtual and real corrections reveal the presence of large logarithmic QED effects of the form  $\alpha L/\pi \equiv (\alpha/\pi) \log(Q^2/m_e^2)$  with  $Q^2 \gg m_e^2$ . They arise when photons or light fermions are radiated off in the direction of incoming or outgoing light particles. In the case of W-pair production the only terms of this sort originate from initial-state photon emission. Radiation of photons from the final-state W bosons can only lead to

$\sqrt{s}$ [GeV]	Born + $\mathcal{O}(\alpha)$	+ h.o.t. for $Q^2 = s$		+ h.o.t. for $Q^2 = s \frac{1-\beta}{1+\beta}$	
		$\mathcal{O}(\alpha^2)$ LL	exp. LL	$\mathcal{O}(\alpha^2)$ LL	exp. LL
161.0	$2.472 \pm 0.001$	3.103	3.003	3.095	2.998
165.0	$8.581 \pm 0.003$	9.079	9.049	9.061	9.033
170.0	$12.270 \pm 0.004$	12.583	12.585	12.567	12.568
175.0	$14.465 \pm 0.004$	14.654	14.670	14.642	14.656
184.0	$16.613 \pm 0.005$	16.668	16.693	16.663	16.686
190.0	$17.257 \pm 0.006$	17.259	17.286	17.259	17.283
205.0	$17.677 \pm 0.006$	17.613	17.638	17.620	17.641

Table 5: Unpolarized total cross-section, given in pb, including radiative electroweak  $\mathcal{O}(\alpha)$  corrections and higher-order terms in the leading-log approximation. These higher-order terms are given with and without soft-photon exponentiation for two different ‘natural’ scale choices.

sizeable corrections if the energy of the W bosons is much larger than their mass. The leading large logarithmic corrections can be calculated by using the so-called structure-function method [16] in leading-log (LL) approximation, i.e. only taking along the terms  $\propto (\alpha L/\pi)^n$ . This procedure also allows the inclusion of soft-photon effects to all orders by means of exponentiation and is discussed in detail in appendix A.

In table 5 the higher-order effects related to the large logarithmic QED corrections are displayed. The  $\mathcal{O}(\alpha^2)$  LL entry contains, in addition to the full  $\mathcal{O}(\alpha)$  result, the contribution from  $\mathcal{O}(\alpha^2)$  LL corrections using  $\hat{\sigma}_0 = \sigma_{\text{Born}}$  in the convolution (68). The exp. LL entry contains on top of that the exponentiation of soft-photon effects. Compared with the full  $\mathcal{O}(\alpha)$  results we observe large  $\mathcal{O}(\alpha^2)$  LL effects near threshold, e.g. 25% at  $\sqrt{s} = 161$  GeV, and moderate ones when sufficiently far above threshold, i.e.  $< 1\%$  for energies above roughly 175 GeV. The additional soft-photon exponentiation is only sizeable near threshold, e.g.  $-4\%$  at  $\sqrt{s} = 161$  GeV. Note that finite-W-width effects will smoothen the threshold behaviour and hence reduce the size of the  $\mathcal{O}(\alpha^2)$  LL effects, nevertheless they will stay sizeable near threshold. The dependence of the higher-order LL corrections [beyond  $\mathcal{O}(\alpha)$ ] on the scale choice  $Q^2$  is negligible, since all natural scales are roughly equal close to threshold. When comparing the popular scale choice  $Q^2 = s$  with  $Q^2 = s(1 - \beta)/(1 + \beta)$ , motivated by the behaviour of the total cross-section near threshold and at high energies [9], the differences are at the 0.1% level (0.2–0.3% at  $\sqrt{s} = 161$  GeV).



An additional improvement of the theoretical predictions can be obtained by using an improved Born cross-section in the convolution (68), taking into account corrections related to  $G_\mu$ ,  $\alpha(s)$ ,  $M_H$  etc.<sup>k</sup>

## 2.4 The width of the W boson

Evidently the width of the W boson is a crucial ingredient for the (off-shell) W-pair production cross-section, especially in the threshold region. Moreover, the branching ratios enter the cross-sections for definite fermions in the final state. As at present the width of the W boson is experimentally poorly known, we need a precise theoretical calculation instead in order to obtain adequate theoretical predictions for off-shell W-pair production.

### 2.4.1 The W-boson width in lowest order

The W width is dominated by decays into fermion–antifermion pairs. In lowest order the partial width for the decay of a W boson into two fermions with masses  $m_{f_i}$  and  $m_{f'_j}$  ( $i, j$  denote the generation index and  $f, f'$  stand for u, d or  $\nu, l$ ) is given by

$$\Gamma_{Wf_i f'_j}^{\text{Born}} = N_C^f \frac{\alpha}{6} \frac{M_W}{2s_W^2} |V_{ij}|^2 \left[ 1 - \frac{m_{f_i}^2 + m_{f'_j}^2}{2M_W^2} - \frac{(m_{f_i}^2 - m_{f'_j}^2)^2}{2M_W^4} \right] \times \frac{\sqrt{(M_W^2 - (m_{f_i} + m_{f'_j})^2)(M_W^2 - (m_{f_i} - m_{f'_j})^2)}}{M_W^2}. \quad (37)$$

For leptonic decays the mixing matrix is diagonal ( $V_{ij} = \delta_{ij}$ ) and the colour factor  $N_C^f$  equals one. For decays into quarks there is a non-trivial quark mixing matrix and  $N_C^f = 3$ . For the quark mixing matrix we have used  $s_{12} = 0.221$ ,  $s_{23} = 0.04$ , and  $s_{13} = 0.004$  [26]. The total width is obtained as a sum over the partial fermionic decay widths with  $m_{f_i} + m_{f'_j} < M_W$

$$\Gamma_W^{\text{Born}} = \sum_{i,j} \Gamma_{Wu_i d_j}^{\text{Born}} + \sum_i \Gamma_{W\nu_i l_i}^{\text{Born}}. \quad (38)$$

As the quark masses are small compared with  $M_W$ , the fermion-mass effects are small for the W decay. If we neglect them we obtain the simple formulae

$$\Gamma_{Wf_i f'_j}^{\text{Born}} = N_C^f \frac{\alpha}{6} \frac{M_W}{2s_W^2} |V_{ij}|^2, \quad \Gamma_W^{\text{Born}} \approx \frac{3\alpha}{2} \frac{M_W}{2s_W^2}. \quad (39)$$

---

<sup>k</sup>As the finite decay width of the W bosons will have a substantial impact on the Coulomb singularity, a LL analysis involving this Coulomb singularity only makes sense for off-shell W bosons.

$M_{\text{H}}$ [GeV]	300	300	300	60	300	1000
$\alpha_s$	0.117	0.123	0.129	0.123	0.123	0.123
$m_t$ [GeV]	164.80	165.26	165.73	148.14	165.26	181.20
$\Gamma_{\text{W}}^{\text{Born}}$ [GeV]	1.9490	1.9490	1.9490	1.9490	1.9490	1.9490
$\bar{\Gamma}_{\text{W}}^{\text{Born}}$ [GeV]	2.0354	2.0354	2.0354	2.0354	2.0354	2.0354
$\Gamma_{\text{W}}$ [GeV]	2.0642	2.0663	2.0684	2.0681	2.0663	2.0639
$\bar{\Gamma}_{\text{W}}$ [GeV]	2.0791	2.0817	2.0844	2.0813	2.0817	2.0819
$\delta_{\text{ew}}$	0.03416	0.03398	0.03380	0.03491	0.03398	0.03275
$\bar{\delta}_{\text{ew}}$	-0.00347	-0.00347	-0.00347	-0.00369	-0.00347	-0.00341
$\delta_{\text{QCD}}$	0.02495	0.02623	0.02751	0.02623	0.02623	0.02623

Table 6: Higgs-mass and  $\alpha_s$  dependence of the W-boson width

### 2.4.2 Higher-order corrections to the W-boson width

The electroweak and QCD radiative corrections for decays into massless fermions ( $m_f \ll M_{\text{W}}$ ) have been calculated in [17]–[19]. The full one-loop electroweak and QCD corrections, together with the complete photonic and gluonic bremsstrahlung, were evaluated for arbitrary fermion masses in [20]. The various calculations are in good agreement. The relative corrections to the total W-boson decay width are given in table 6. The electroweak corrections in the on-shell scheme  $\delta^{\text{ew}} \equiv \Gamma_{\text{W}}/\Gamma_{\text{W}}^{\text{Born}} - 1 - \delta^{\text{QCD}}$  are predominantly originating from the running of  $\alpha$  and the corrections  $\propto \alpha m_t^2/M_{\text{W}}^2$  to the  $\rho$  parameter. These corrections can be easily accounted for by parametrizing the lowest-order width in terms of  $G_{\mu}$  and  $M_{\text{W}}$  instead of  $\alpha$  and  $s_{\text{W}}^2$ . The width in this  $G_{\mu}$  parametrization  $\bar{\Gamma}_{\text{W}}$  is related to the width in the on-shell parametrization  $\Gamma_{\text{W}}$  by

$$\begin{aligned}
\bar{\Gamma}_{\text{W}} &= \frac{\Gamma_{\text{W}} - \Gamma_{\text{W}}^{\text{Born}} \Delta r^{1\text{-loop}}}{1 - \Delta r} = \Gamma_{\text{W}}^{\text{Born}} \frac{1 + \delta^{\text{ew}} + \delta^{\text{QCD}} - \Delta r^{1\text{-loop}}}{1 - \Delta r} \\
&= \bar{\Gamma}_{\text{W}}^{\text{Born}} (1 + \delta^{\text{ew}} + \delta^{\text{QCD}} - \Delta r^{1\text{-loop}}) \equiv \bar{\Gamma}_{\text{W}}^{\text{Born}} (1 + \bar{\delta}^{\text{ew}} + \delta^{\text{QCD}}). \tag{40}
\end{aligned}$$

As can be seen from table 6 the electroweak corrections with respect to the parametrization with  $G_{\mu}$ ,  $\bar{\delta}^{\text{ew}}$ , depend in a negligible way on  $M_{\text{H}}$ , and remain below 0.5% for the total width. The QCD corrections  $\delta^{\text{QCD}}$  are practically constant and equal to  $2\alpha_s(M_{\text{W}}^2)/(3\pi)$ , their value for zero fermion masses. For the numerical evaluation we use  $\alpha_s(M_{\text{W}}^2) = 0.123$  (i.e. equal to the default input value). The difference between  $\Gamma_{\text{W}}$  and the more precise  $\bar{\Gamma}_{\text{W}}$  is caused by missing higher-order terms related to  $\Delta r$ .

We obtain the following improved Born approximation for the total and partial widths [40]

$$\Gamma_{\text{W}\nu_i l_i} \approx \bar{\Gamma}_{\text{W}\nu_i l_i}^{\text{Born}} = \frac{G_{\mu} M_{\text{W}}^3}{6\sqrt{2}\pi},$$

	Born $m_f \neq 0$	complete $m_f \neq 0$	complete $m_f = 0$	IBA ( $m_f = 0$ )	Branching ratio
$\Gamma(W \rightarrow e\nu_e)$	0.2262	0.2255	0.2255	0.2262	0.1083
$\Gamma(W \rightarrow \mu\nu_\mu)$	0.2262	0.2255	0.2255	0.2262	0.1083
$\Gamma(W \rightarrow \tau\nu_\tau)$	0.2261	0.2253	0.2255	0.2262	0.1082
$\Gamma(W \rightarrow \text{lep.})$	0.6785	0.6763	0.6765	0.6787	0.3249
$\Gamma(W \rightarrow ud)$	0.6455	0.6684	0.6684	0.6708	0.3211
$\Gamma(W \rightarrow us) \times 10$	0.3315	0.3432	0.3432	0.3444	0.0165
$\Gamma(W \rightarrow ub) \times 10^4$	0.1080	0.1122	0.1124	0.1128	0.000005
$\Gamma(W \rightarrow cd) \times 10$	0.3312	0.3431	0.3432	0.3444	0.0165
$\Gamma(W \rightarrow cs)$	0.6441	0.6672	0.6673	0.6697	0.3205
$\Gamma(W \rightarrow cb) \times 10^2$	0.1080	0.1121	0.1124	0.1128	0.0005
$\Gamma(W \rightarrow \text{had.})$	1.3569	1.4054	1.4055	1.4104	0.6751
$\Gamma(W \rightarrow \text{all})$	2.0354	2.0817	2.0820	2.0891	

Table 7: Partial and total W-decay widths  $\bar{\Gamma}_W$  in different approximations given in GeV.

$$\begin{aligned}
\Gamma_{Wu_i d_j} &\approx \bar{\Gamma}_{Wu_i d_j}^{\text{Born}} \left( 1 + \frac{\alpha_s(M_W^2)}{\pi} \right) = \frac{G_\mu M_W^3}{2\sqrt{2}\pi} |V_{ij}|^2 \left( 1 + \frac{\alpha_s(M_W^2)}{\pi} \right), \\
\Gamma_W &\approx \bar{\Gamma}_W^{\text{Born}} \left( 1 + \frac{2\alpha_s(M_W^2)}{3\pi} \right) = \frac{3G_\mu M_W^3}{2\sqrt{2}\pi} \left( 1 + \frac{2\alpha_s(M_W^2)}{3\pi} \right).
\end{aligned} \tag{41}$$

In table 7 we compare the improved Born approximation (IBA) for the partial and total widths, given by equation (41), with the lowest-order widths, the widths including the complete first-order and leading higher-order corrections for finite fermion masses, and the same for vanishing fermion masses, all in the  $G_\mu$  parametrization. The effects of the fermion masses, which are of the order  $m_f^2/M_W^2$ , are below 0.3%. Consequently the exact numerical values for the masses of the external fermions are irrelevant. The IBA reproduces the exact results within 0.4% (0.6% for the decays into a b-quark). The branching ratios for the individual decay channels derived from equation (41), which depend only on  $\alpha_s$  and  $V_{ij}$ , agree numerically within 0.1% with those obtained from the full one-loop results.

### 3 Off-Shell W-Pair Production

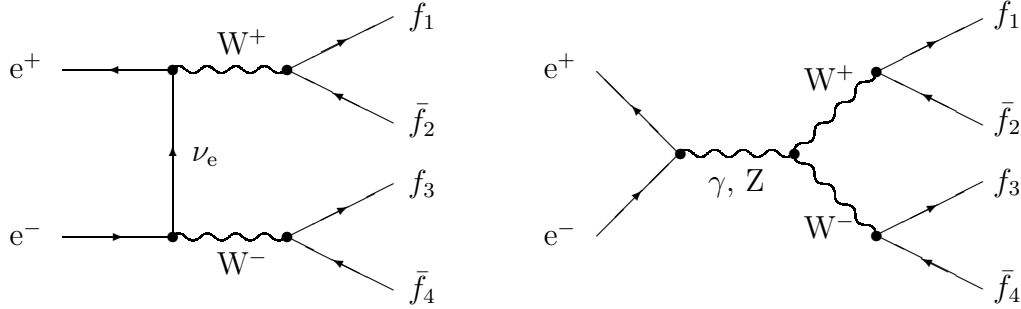


Figure 4: Lowest-order diagrams for  $e^+e^- \rightarrow W^+W^- \rightarrow 4f$

	$\bar{d}u$	$\bar{s}c$	$\bar{e}\nu_e$	$\bar{\mu}\nu_\mu$	$\bar{\tau}\nu_\tau$
$d\bar{u}$	$4\mathcal{3}$	<b>11</b>	20	<b>10</b>	<b>10</b>
$e\bar{\nu}_e$	20	20	$5\mathcal{6}$	18	18
$\mu\bar{\nu}_\mu$	<b>10</b>	<b>10</b>	18	$19$	<b>9</b>

Table 8: Number of Feynman diagrams for W-pair produced four-fermion final states.

### 3.1 Lowest order: an introduction

So far we have only considered the production of stable W bosons. This is, however, only an approximation and in particular in the threshold region it is not sufficient. Rather, one has to describe the W bosons as resonances, with a finite width so as to avoid singularities inside the physical phase space, and analyse their presence through their decay products:

$$e^+ + e^- \rightarrow W^+ + W^- \rightarrow f_1 + \bar{f}_2 + f_3 + \bar{f}_4. \quad (42)$$

Process (42) involves two resonant W bosons (doubly-resonant) and can be viewed as a very natural first step beyond the on-shell limit. In lowest order this process is represented by the three Feynman diagrams shown in figure 4. However, the full four-fermion process does not only proceed through the three doubly-resonant diagrams. There are also contributions from other diagrams with the same initial and final states, but different intermediate states. Classifications of four-fermion production processes and of the contributing diagrams are given in [41, 42]. In table 8 we give the number of diagrams contributing for final states that can be reached by W-pair intermediate states. These so-called charged-current processes are sometimes referred to as  $CCn$ , with  $n$  denoting the number of contributing diagrams [e.g.  $CC3$  denotes process (42)]. The simplest case (**boldface** numbers in table 8) is fully covered by doubly- and singly-resonant diagrams as given in figures 4 and 5. Additional graphs of the types shown in figure 6 must be taken into account if electrons or electron-neutrinos are produced (roman numbers in table 8). If the produced final state consists of particle–antiparticle pairs, the final state can also be obtained through intermediate Z-pair production, leading to extra Feynman diagrams

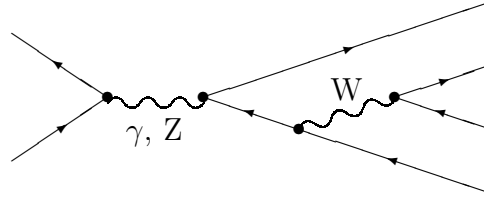


Figure 5: Example of a singly-resonant diagram.

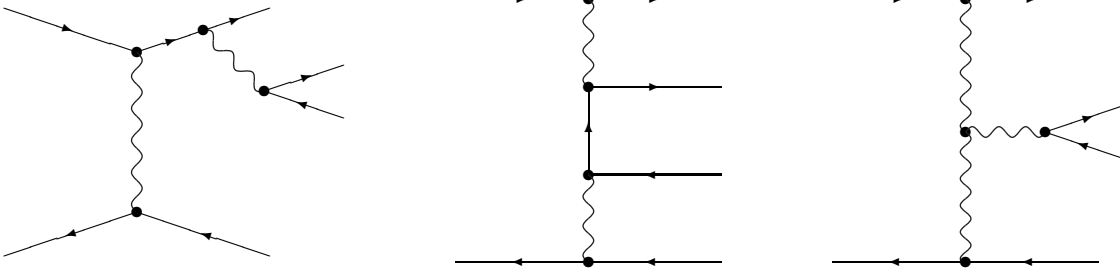


Figure 6: Examples of additional diagrams for final states with electrons and electron-neutrinos.

(*italic* numbers in table 8). Finally, it should be mentioned that QCD diagrams, involving an intermediate gluon, contribute in the case of final states consisting of two quark–antiquark pairs.

### 3.2 Semi-analytical approach

We will now, in a first step of sophistication beyond on-shell W-pair production, introduce a finite W width and perform the CC3 calculation. In the following a semi-analytical method will be emphasized, whereas Monte Carlo methods are treated elsewhere [22]. The starting point is

$$\sigma^{\text{CC3}}(s) = \int_0^s ds_+ \rho_W(s_+) \int_0^{(\sqrt{s}-\sqrt{s_+})^2} ds_- \rho_W(s_-) \sigma_0^{\text{CC3}}(s; s_+, s_-), \quad (43)$$

with  $s_+ = k_+^2$  and  $s_- = k_-^2$  the virtualities of the internal W bosons. The Breit-Wigner densities

$$\rho_W(s_\pm) = \frac{1}{\pi} \frac{M_W \Gamma_W}{|s_\pm - M_W^2 + iM_W \Gamma_W|^2} \times \text{BR} \quad (44)$$

contain the finite width of the W boson, the coupling constants of its decay to fermions, and the corresponding branching ratio. In the limit of stable W bosons, the on-shell cross-section is recovered via

$$\rho_W(s_\pm) \xrightarrow{\Gamma_W \rightarrow 0} \delta(s_\pm - M_W^2) \times \text{BR}. \quad (45)$$

The two-fold differential cross-section contains terms corresponding to the Feynman diagrams of figure 4 and their interferences. In the notation of [43] it may be described by three terms,

$$\sigma_0^{\text{CC3}}(s; s_+, s_-) = \frac{(G_\mu M_W^2)^2}{8\pi s} \left[ \mathcal{C}_{\text{CC3}}^s \mathcal{G}_{\text{CC3}}^{33} + \mathcal{C}_{\text{CC3}}^{st} \mathcal{G}_{\text{CC3}}^{3f} + \mathcal{C}_{\text{CC3}}^t \mathcal{G}_{\text{CC3}}^{ff} \right]. \quad (46)$$

The couplings  $\mathcal{C}_{\text{CC3}}^{s,st,t}$  contain the weak mixing angle, the Z-e vector and axial-vector coupling, the triple-gauge-boson couplings, and the  $s$ -channel Z and  $\gamma$  propagators. The kinematical functions  $\mathcal{G}_{\text{CC3}}^{33,3f,ff}$  are known analytically [21]:

$$\mathcal{G}_{\text{CC3}}^{ff}(s; s_+, s_-) = \frac{1}{48} \left[ \lambda(s, s_+, s_-) + 12 s (s_+ + s_-) - 48 s_+ s_- + 24 s_+ s_- (s - s_+ - s_-) \mathcal{L}(s; s_+, s_-) \right], \quad (47)$$

$$\mathcal{G}_{\text{CC3}}^{33}(s; s_+, s_-) = \frac{\lambda(s, s_+, s_-)}{192} \left[ \lambda(s, s_+, s_-) + 12 (s s_+ + s s_- + s_+ s_-) \right], \quad (48)$$

$$\mathcal{G}_{\text{CC3}}^{3f}(s; s_+, s_-) = \frac{1}{48} \left\{ (s - s_+ - s_-) \left[ \lambda(s, s_+, s_-) + 12 s (s s_+ + s s_- + s_+ s_-) \right] - 24 s_+ s_- (s s_+ + s s_- + s_+ s_-) \mathcal{L}(s; s_+, s_-) \right\}, \quad (49)$$

where

$$\lambda(s, s_+, s_-) = s^2 + s_+^2 + s_-^2 - 2 s s_+ - 2 s s_- - 2 s_+ s_-, \quad (50)$$

$$\mathcal{L}(s; s_+, s_-) = \frac{1}{\sqrt{\lambda(s, s_+, s_-)}} \log \left( \frac{s - s_+ - s_- + \sqrt{\lambda(s, s_+, s_-)}}{s - s_+ - s_- - \sqrt{\lambda(s, s_+, s_-)}} \right). \quad (51)$$

The numerical importance of the W-boson off-shellness in equation (43) is displayed in figure 7. Clearly, the effect of the finite W width is comparable to the one from universal initial-state radiation, defined in section 3.4.1.

The second level of sophistication of W-pair production is reached by performing calculations for complete sets of Feynman diagrams for specific final states. The simplest case, the **CC11** class of processes, corresponds to four-fermion final states without electrons or electron-neutrinos and without particle-antiparticle pairs. The corresponding gauge-invariant set of Feynman diagrams consists of the three doubly-resonant diagrams of figure 4 plus at most eight singly-resonant diagrams of the type shown in figure 5. This class of processes is still calculable in the semi-analytical approach and is of specific interest for the W-mass determination and the TGC studies. The corresponding cross-section is given by [43]

$$\sigma^{\text{CC11}}(s) = \int ds_+ \int ds_- \frac{\sqrt{\lambda(s, s_+, s_-)}}{\pi s^2} \sum_{k=1}^{15} \frac{d^2 \sigma_k(s, s_+, s_-)}{ds_+ ds_-} \quad (52)$$

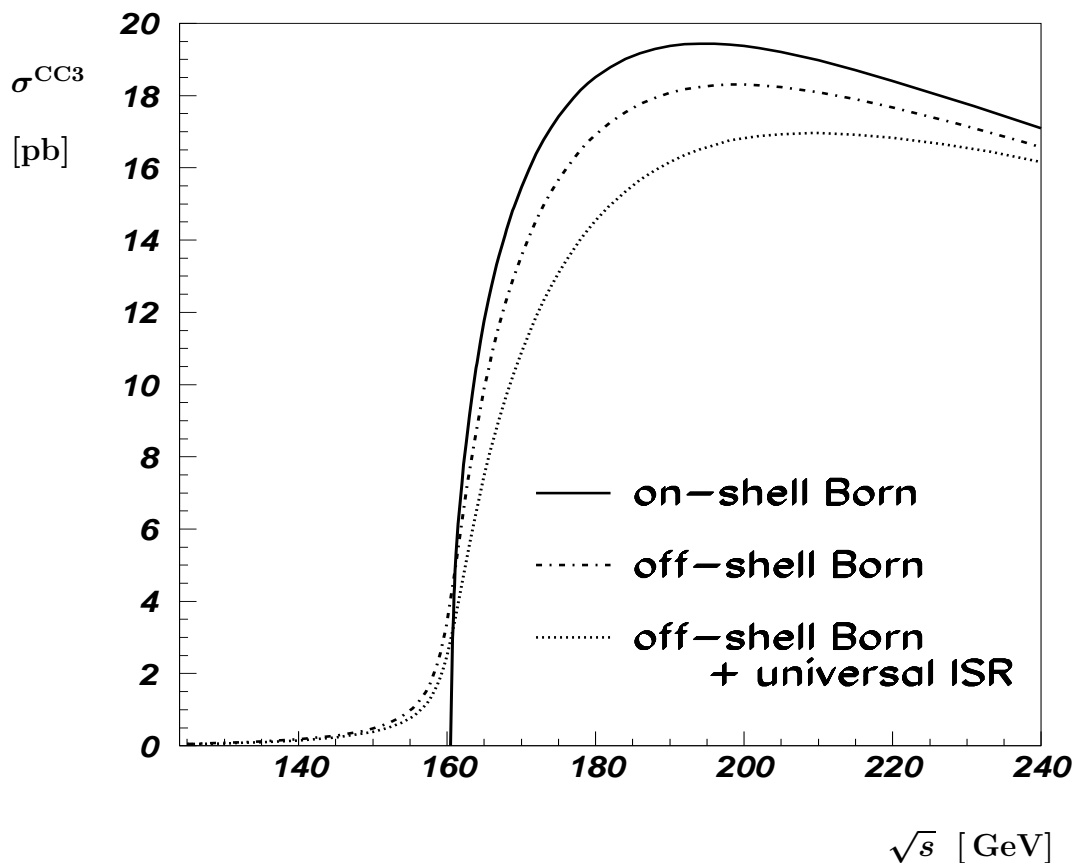


Figure 7: The inclusive CC3 cross-section.

with

$$\frac{d^2\sigma_k}{ds_+ ds_-} = \mathcal{C}_k \mathcal{G}_k(s, s_+, s_-). \quad (53)$$

Initial- and final-state couplings, as well as intermediate W, Z, and  $\gamma$  propagators are collected in the  $\mathcal{C}_k$ 's. The kinematical details are contained in the  $\mathcal{G}_k$ 's. Because of symmetry properties, under the exchanges of the three virtualities, only six of these kinematical functions are independent. Apart from the three kinematical functions of the CC3 process, three more enter as a result of the singly-resonant diagrams. Explicit expressions can be found in [43].

A similar semi-analytical analysis of the remaining four-fermion final states has not been performed so far, although this would be desirable.

### 3.3 Lowest order: the gauge-invariance issue

The discussion in the previous subsections has avoided the question of gauge invariance which arises when going from on-shell W-pair production to the off-shell case. There are two sources of gauge non-invariance one has to be aware of.

First of all there is the issue of gauge non-invariance as a result of incomplete sets of contributions. Consider to this end again the process

$$e^+ + e^- \rightarrow W^+ + W^- \rightarrow f_1 + \bar{f}_2 + f_3 + \bar{f}_4, \quad (54)$$

represented by the three Feynman diagrams shown in figure 4. Forgetting about the finite W width the corresponding matrix element can be written in the following form:

$$\begin{aligned} \widehat{\mathcal{M}}_{\text{Born}}^\kappa &= \left[ \delta_{\kappa-} \frac{e^2}{2s_W^2} \mathcal{M}_I^{\kappa,\rho\sigma} + e^2 \mathcal{M}_Q^{\kappa,\rho\sigma} \right] \\ &\times \frac{1}{k_+^2 - M_W^2} \times \frac{e}{\sqrt{2}s_W} \bar{u}_1 \gamma_\rho \omega_- v_2 \times \frac{1}{k_-^2 - M_W^2} \times \frac{e}{\sqrt{2}s_W} \bar{u}_3 \gamma_\sigma \omega_- v_4, \end{aligned} \quad (55)$$

where

$$\begin{aligned} \mathcal{M}_Q^{\kappa,\rho\sigma} &= \frac{2M_Z^2}{s(s - M_Z^2)} \bar{v}_+ \left[ \not{k}_+ g^{\rho\sigma} - \gamma^\rho k_+^\sigma + \gamma^\sigma k_-^\rho \right] \omega_\kappa u_-, \\ \mathcal{M}_I^{\kappa,\rho\sigma} &= \frac{1}{t} \bar{v}_+ \gamma^\rho (\not{k}_+ - \not{p}_+) \gamma^\sigma \omega_\kappa u_- - \frac{s}{M_Z^2} \mathcal{M}_Q^{\kappa,\rho\sigma} \end{aligned} \quad (56)$$

are directly related to the corresponding on-shell quantities  $\mathcal{M}_I$  and  $\mathcal{M}_Q$  defined in equation (15). Here  $k_\pm$  are the momenta of the  $W^\pm$  bosons as reconstructed from the decay products, and  $s$  and  $t$  the usual Mandelstam variables for  $e^+e^- \rightarrow W^+W^-$ . We have assumed that all fermion masses are negligible. In a renormalizable gauge such as a  $R_\xi$  gauge one would otherwise have to consider in addition diagrams involving one or two unphysical charged Higgs bosons instead of the W bosons.

Whereas for on-shell W bosons the contributions of  $\mathcal{M}_I$  and  $\mathcal{M}_Q$  are separately gauge-invariant, for off-shell W bosons not even  $\widehat{\mathcal{M}}_{\text{Born}}$  is gauge-invariant. This can be illustrated by considering the doubly-resonant diagrams in an axial gauge [9]. To this end we replace the conventional 't Hooft–Feynman gauge-fixing term for the W boson by  $-(n^\mu W_\mu^+)(n^\nu W_\nu^-)$ . This modifies the W-boson propagators in the diagrams of figure 4 and, since this gauge-fixing term does not eliminate the mixing between the W-boson field and the corresponding unphysical Higgs field, leads to mixing propagators between those fields, giving rise to additional Feynman diagrams. Combining all relevant diagrams yields the following extra contribution to  $\widehat{\mathcal{M}}_{\text{Born}}^\kappa$  in the axial gauge:

$$\begin{aligned} \widehat{\mathcal{M}}_{\text{Born}}^\kappa \Big|_{\text{axial gauge}} - \widehat{\mathcal{M}}_{\text{Born}}^\kappa \Big|_{\text{'t Hooft–Feynman gauge}} &= e^2 \left[ \delta_{\kappa-} \frac{1}{2s_W^2} - \frac{M_Z^2}{s} \right] \frac{1}{s - M_Z^2} \bar{v}_+ \gamma_\mu \omega_\kappa u_- \\ &\times \left[ \frac{g^{\mu\rho} n^\sigma}{(k_-^2 - M_W^2)(n \cdot k_-)} - \frac{g^{\mu\sigma} n^\rho}{(k_+^2 - M_W^2)(n \cdot k_+)} \right] \times \frac{e}{\sqrt{2}s_W} \bar{u}_1 \gamma_\rho \omega_- v_2 \times \frac{e}{\sqrt{2}s_W} \bar{u}_3 \gamma_\sigma \omega_- v_4. \end{aligned} \quad (57)$$



Note that these gauge-dependent terms involve either a pole in  $(k_+^2 - M_W^2)$  or  $(k_-^2 - M_W^2)$  but not both, i.e. they are only singly-resonant. These terms are exactly cancelled by the gauge-dependent contributions of eight singly-resonant diagrams contributing to the same final state with the topology shown in figure 5.

The sum of the doubly-resonant diagrams and the singly-resonant ones with the topology shown in figure 5 is in general gauge-invariant. This follows directly from the fact that for final states with four different fermions and no electrons or positrons those diagrams are the only ones that contribute. As a consequence the non-resonant diagrams are not needed to cancel the gauge-dependent terms of the doubly-resonant diagrams. Among the non-resonant diagrams and the singly-resonant ones that do not have the topology shown in figure 5 further gauge-invariant subsets can be identified by considering other four-fermion final states.

Thus, in general all graphs that contribute to a given final state have to be taken into account and one is lead to consider the complete process  $e^+e^- \rightarrow 4f$ , including all resonant and non-resonant graphs, in order to obtain a manifestly gauge-independent result.

Simple estimates indicate that all non-doubly-resonant contributions are typically suppressed by a factor  $\Gamma_W/M_W \approx 2.5\%$  on the cross-section level for each non-resonant W propagator<sup>l</sup>. This is confirmed by explicit calculations [22]. For instance, using covariant ( $R_\xi$ ) gauges the universal non-doubly-resonant graphs that occur for all final states (see figure 5) contribute less than 0.15% to the total cross-section for  $175 \text{ GeV} < \sqrt{s} < 205 \text{ GeV}$ , and 0.3% at 161 GeV. The contribution of the non-doubly-resonant  $t$ -channel photon-exchange graphs, which only occur when there are electrons in the final state, depends very much on the angular cut imposed on the outgoing electrons; for  $10^\circ$  they contribute at the per-cent level, e.g.  $\sim 4\%$  at  $\sqrt{s} = 190 \text{ GeV}$ . Although all these non-doubly-resonant contributions are suppressed, they should nevertheless be taken into account to reach a theoretical accuracy of  $\sim 0.5\%$ . Finally, the QCD graphs have been shown not to interfere with the electroweak graphs to any sizable extent, and can thus be computed using standard (Monte Carlo) QCD programs.

Even when considering the complete set of graphs contributing to a given final state, there is still a more fundamental gauge-invariance problem to be solved. The resonant graphs discussed above involve poles at  $k_\pm^2 = M_W^2$ .<sup>m</sup> These have to be cured by introducing the finite width in one way or another, while at the same time preserving gauge independence and, through a proper energy dependence, unitarity. In field theory, such widths arise naturally from the imaginary parts of higher-order diagrams describing the boson self-energies, resummed to all orders. This procedure has been used with great success in the past: indeed, the Z resonance can be described to very high numerical accuracy. However, in doing a Dyson summation of self-energy graphs, we are singling out only a very limited subset of all the possible higher-order

---

<sup>l</sup>For differential distributions that do not involve an explicit phase, like e.g.  $\sigma_{\text{tot}}$  or  $d\sigma/(d\cos\theta)$ , there will be no interference between doubly- and singly-resonant diagrams. Consequently the non-doubly-resonant contributions are suppressed by  $\Gamma_W^2/M_W^2 \approx 0.1\%$  in those cases [44].

<sup>m</sup>There are similar poles associated with diagrams containing internal Z propagators. These correspond to Z-pair production and are here considered as background to W-pair production.

diagrams. It is therefore not surprising that one often ends up with a result that retains some gauge dependence.

For example it is very tempting to systematically replace  $1/(q^2 - M^2)$  by  $1/(q^2 - M^2 + iM\Gamma)$ , also for  $q^2 < 0$ . Here  $\Gamma$  denotes the physical width of the particle with mass  $M$  and momentum  $q$ . This is the so-called ‘fixed-width scheme’. As in general the resonant diagrams are not gauge-invariant by themselves, this substitution will again destroy gauge invariance. Moreover, the ‘fixed-width scheme’ has no physical motivation. In perturbation theory the propagator for space-like momenta does not develop an imaginary part. Consequently, unitarity is violated in this scheme. To improve on the latter the constant width could be replaced by a running one. This can, however, not cure the gauge non-invariance problem. At this point one might ask oneself the legitimate question whether the gauge breaking occurring in the ‘fixed-width scheme’ is numerically relevant or, like the gauge breaking in the LEP1 analyses, negligible for all practical purposes. Of course, such a statement can only be made on the basis of an explicit comparison with truly gauge-invariant schemes in the full LEP2 energy range. We will come back to that point later on, after having defined a scheme that is gauge-invariant and reliable at LEP2.

Below we will list a few ways to come to a gauge-invariant result and discuss their validity.

One way to sidestep the gauge non-invariance problem is by simply multiplying the full matrix element by  $[q^2 - M^2]/[q^2 - M^2 + iM\Gamma(q^2)]$ , which is evidently gauge-invariant [45, 46]. In this way the pole at  $q^2 = M^2$  is softened into a resonance, at the expense of mistreating the non-resonant parts. It should be noted that when the doubly-resonant diagrams are not dominant, like at energies at and below the W-pair production threshold, this so-called ‘fudge-factor scheme’ can lead to large deviations [47].

The second possibility is the so-called ‘pole scheme’ [23]–[25]. In this scheme one decomposes the complete amplitude, consisting of contributions from doubly-resonant diagrams  $R_{+-}$  (corresponding in lowest order to  $\widehat{\mathcal{M}}_{\text{Born}}$ ), singly-resonant diagrams  $R_+$ ,  $R_-$ , and non-resonant diagrams  $N$ , according to their poles as follows:

$$\begin{aligned}
\mathcal{M} &= \frac{R_{+-}(k_+^2, k_-^2, \theta)}{(k_+^2 - M_W^2)(k_-^2 - M_W^2)} + \frac{R_+(k_+^2, k_-^2, \theta)}{k_+^2 - M_W^2} + \frac{R_-(k_+^2, k_-^2, \theta)}{k_-^2 - M_W^2} + N(k_+^2, k_-^2, \theta) \\
&= \frac{R_{+-}(M_W^2, M_W^2, \theta)}{(k_+^2 - M_W^2)(k_-^2 - M_W^2)} \\
&\quad + \frac{1}{k_+^2 - M_W^2} \left[ \frac{R_{+-}(M_W^2, k_-^2, \theta) - R_{+-}(M_W^2, M_W^2, \theta)}{k_-^2 - M_W^2} + R_+(M_W^2, k_-^2, \theta) \right] \\
&\quad + \frac{1}{k_-^2 - M_W^2} \left[ \frac{R_{+-}(k_+^2, M_W^2, \theta) - R_{+-}(M_W^2, M_W^2, \theta)}{k_+^2 - M_W^2} + R_-(k_+^2, M_W^2, \theta) \right] \\
&\quad + \left[ \frac{R_{+-}(k_+^2, k_-^2, \theta) + R_{+-}(M_W^2, M_W^2, \theta) - R_{+-}(M_W^2, k_-^2, \theta) - R_{+-}(k_+^2, M_W^2, \theta)}{(k_+^2 - M_W^2)(k_-^2 - M_W^2)} \right. \\
&\quad \left. + \frac{R_+(k_+^2, k_-^2, \theta) - R_+(M_W^2, k_-^2, \theta)}{k_+^2 - M_W^2} \right]
\end{aligned}$$

$$+ \frac{R_-(k_+^2, k_-^2, \theta) - R_-(k_+^2, M_W^2, \theta)}{k_-^2 - M_W^2} + N(k_+^2, k_-^2, \theta) \Big]. \quad (58)$$

Here  $\theta$  stands generically for all angular variables which should be defined in such a way that their integration boundaries are independent of  $k_+^2$  and  $k_-^2$ . Otherwise these angular variables would introduce an additional dependence on  $k_+^2$  and  $k_-^2$ , and the correct pole terms could only be extracted after the angular integrations had been performed. This would complicate the pole decomposition and, in particular, would not be suited for a Monte-Carlo generator. Appropriate variables are e.g. the angles in the  $e^+e^-$ -CM system but not the Mandelstam variables. In equation (58)  $\mathcal{M}$  is decomposed into gauge-invariant subsets originating from double-pole terms, single-pole terms, and non-pole terms (with respect to  $M_W$ ). Introducing now the finite width only in the pole factors and not in the finite constant residues in brackets does not destroy gauge invariance. We note that different ways of introducing the finite width, e.g. constant or running, differ only by terms that are of higher-order and/or that are not of the double-pole type<sup>n</sup>. The same holds for different choices of the angular variables  $\theta$  (see section 3.4.4).

A drawback of the ‘pole scheme’ is the fact that it is not defined below the W-pair production threshold and that it yields unreliable results just above this threshold (see section 3.4.4).

Apart from yielding gauge-invariant results, the ‘pole-scheme’ decomposition also constitutes a systematic expansion according to the degree of resonance, i.e. in powers of  $\Gamma_W/(M_W\beta)$ . Here the enhancement factor  $1/\beta$  represents the influence of the nearby threshold on the expansion. Sufficiently far above the W-pair threshold and after imposing appropriate angular and invariant mass cuts, in order to reduce Z-pair and  $t$ -channel photon-exchange backgrounds, the cross-section for off-shell W-pair production is dominated by (or may even be defined by) the double-pole terms  $R_{+-}(M_W^2, M_W^2, \theta)$ . At least at lowest order these may be related to on-shell W-pair production in the following way:

$$R_{+-}(M_W^2, M_W^2, \theta) = \sum_{\lambda_+, \lambda_-} \mathcal{M}_{e^+e^- \rightarrow W^+W^-}^{\lambda_+, \lambda_-} \times \mathcal{M}_{W^+ \rightarrow f_1\bar{f}_2}^{\lambda_+} \times \mathcal{M}_{W^- \rightarrow f_3\bar{f}_4}^{\lambda_-}, \quad (59)$$

where  $\mathcal{M}_{e^+e^- \rightarrow W^+W^-}$ ,  $\mathcal{M}_{W^+ \rightarrow f_1\bar{f}_2}$ ,  $\mathcal{M}_{W^- \rightarrow f_3\bar{f}_4}$  denote the matrix elements for the production of two on-shell W bosons and their subsequent decay into fermion–antifermion pairs. As such the ‘pole scheme’ is a natural starting point for the systematic evaluation of higher-order corrections [9, 25] (see also section 3.4.4).

As a third method, one may determine the minimal set of Feynman diagrams that is necessary to compensate for the gauge violation caused by the self-energy graphs, and try to include these [48, 49]. This is obviously the theoretically most satisfying solution, but it may cause

---

<sup>n</sup>There is no unique prescription for the propagator including the finite width. Instead of the constant term  $M_W\Gamma_W$  one can also use a width depending on the invariant mass  $k_\pm^2$ . This corresponds to different definitions of the (renormalized) W mass, which is fixed by the pole of the propagator. A popular choice is  $k^2\Gamma_W/M_W$ , which amounts to a shift in  $M_W$  by  $\Gamma_W^2/(2M_W) \approx 26$  MeV relative to the propagator with the constant-width term.

an increase in the complexity of the matrix elements and a consequent slowing down of the numerical calculations. For the vector bosons, the lowest-order widths are given by the imaginary parts of the fermion loops in the one-loop self-energies. It is therefore natural to include the other possible one-particle-irreducible fermionic one-loop corrections [47, 50, 51]. For the process  $e^+e^- \rightarrow 4f$  this amounts to adding the fermionic triple-gauge-boson vertex corrections. The complete set of fermionic contributions form a gauge-independent subset and obey all Ward identities exactly, even with resummed propagators [52]. This implies that the high-energy and collinear limits are properly behaved. In contrast to all other schemes mentioned above, the ‘fermion-loop scheme’ recommended here does not modify the theory by hand but selects an appropriate set of higher-order contributions to restore gauge invariance. To solve the problem of gauge invariance related to the width, we in fact only have to consider the imaginary parts of these fermionic contributions<sup>o</sup>.

The ‘fermion-loop scheme’ should work properly for all tree-level calculations involving resonant W bosons and Z bosons or other particles decaying exclusively into fermions. This also includes, for instance, the hard-photon process  $e^+e^- \rightarrow 4f + \gamma$ , which requires in addition to fermionic vertex corrections also fermionic box corrections. For resonating particles decaying also into bosons, such as the top quark, or for calculating RC’s to  $e^+e^- \rightarrow 4f$ , which also involves bosonic corrections, the ‘fermion-loop scheme’ is not really suited.

Although the latter scheme is well-justified in standard perturbation theory, it should be stressed that any working scheme is arbitrary to a greater or lesser extent: since the Dyson summation must necessarily be taken to all orders of perturbation theory, and we are not able to compute the complete set of *all* Feynman diagrams to *all* orders, the various schemes differ even if they lead to formally gauge-invariant results. In [53] another technique, the so-called ‘pinch technique’, has been introduced in order to construct a gauge-parameter-independent Dyson summation. Even if the ‘pinch technique’ yields gauge-independent results, it still contains some arbitrariness in the sense that one still has the freedom to shift gauge-independent parts that fulfill the Ward identities from the vertex corrections to the self-energies. For instance, it has been demonstrated in [54] that the ‘background-field method’ can be used to construct an infinite variety of such shifts, all representing (theoretically) equally well-justified schemes for resumming self-energies.

Now it is a numerical question how much the predictions of different schemes differ. In [51] a detailed study has been given for the process  $e^+e^- \rightarrow e^-\bar{\nu}_e u\bar{d}$ , a process that is highly sensitive to  $U(1)$  electromagnetic gauge violation. In this process the electron may emit a virtual photon, whose  $k^2$  can be as small as  $m_e^2$ : with a total centre-of-mass energy of  $\sqrt{s}$  available, we have a mass ratio of  $s/m_e^2 = \mathcal{O}(10^{11})$ , large enough to amplify even a tiny gauge violation in a disastrous way<sup>p</sup>. In table 9 we give the cross-section corresponding to the  $t$ -channel photon-exchange diagrams, responsible for the amplification of the gauge-breaking terms in the collinear limit. The results are given for two values of the minimum electron scattering angle

---

<sup>o</sup>As the Ward identities are linear, we can separate the real and imaginary parts.

<sup>p</sup>This was noted already in [55], and investigated further in [46].

$\theta_{\min}$ , displaying the effect of cutting away the dangerous collinear limit. It is clear that a naive introduction of a running width without a proper inclusion of fermionic corrections to the three-vector-boson vertex, which breaks  $U(1)$  electromagnetic gauge invariance, leads to completely unreliable results. The above-described gauge-invariant methods as well as the  $U(1)$ -preserving ‘fixed-width scheme’ numerically deviate by much less than  $\Gamma_W/M_W$ . Hence, a naive running width is not suited for LEP2, whereas a constant width, although  $SU(2) \times U(1)$  gauge breaking, might constitute a workable approach. As in the collinear limit  $k^2 \rightarrow 0$  the gauge-breaking terms originating from a naive running width are proportional to the dominant lowest-order graphs, it is possible to multiply the  $\gamma WW$  Yang-Mills vertex with a simple factor to successfully restore the  $U(1)$  gauge invariance. This factor is, however, certainly not universal. It will depend on the way the running width is introduced and on the process under investigation. Moreover, such a simple factor breaks unitarity and at high energies the full expression from the fermion loops is required for having a proper energy dependence.

Scheme	$\sigma$ [pb]	
	$\theta_{\min} = 0^\circ$	$\theta_{\min} = 10^\circ$
Fixed width	.08887(8)	.01660(3)
Running width, no correction	60738(176)	.01713(3)
Fudge factor, with running width	.08892(8)	.01671(3)
Pole scheme, with running width	.08921(8)	.01666(3)
fermion-loop scheme	.08896(8)	.01661(3)

Table 9: Cross-section in different schemes for the  $t$ -channel photon-exchange diagrams of  $e^+e^- \rightarrow e^-\bar{\nu}_e u\bar{d}$ . All schemes were computed using the same sample, so the differences are much more significant than the integration error suggests.

### 3.4 Radiative corrections

So far no complete treatment for the  $\mathcal{O}(\alpha)$  corrections to off-shell  $W$ -pair production is available. Essentially only the initial-state photonic corrections, the final-state Coulomb correction, and the full hard process  $e^+e^- \rightarrow 4f+\gamma$  have been treated so far<sup>q</sup>. These are discussed in the following. The leading weak effects are normally taken into account through dressed lowest-order matrix elements, using  $G_\mu$  and  $\alpha(s)$ .<sup>r</sup> In addition we describe a general strategy for the calculation of corrections beyond the lowest order using the ‘pole scheme’.

<sup>q</sup>An evaluation of all resummed one-particle-irreducible fermionic  $\mathcal{O}(\alpha)$  corrections, in the context of the ‘fermion-loop scheme’, is in progress [52].

<sup>r</sup>The uncertainty associated with different theoretical definitions of  $s_W^2$ , i.e.  $s_W^2 = 1 - M_W^2/M_Z^2$  or  $s_W^2 = \pi \alpha(4M_W^2)/(\sqrt{2}G_\mu M_W^2)$ , are found to be below 0.1%.

### 3.4.1 Initial-state radiation

Most of the published calculations for corrections to off-shell W-pair production that have been done so far cover only part of the photonic corrections, mainly because these are easily treatable and constitute a large part of the RC's. From the discussion of the on-shell process we know that initial-state radiation (ISR) yields large corrections originating from the leading collinear logarithms. As will be discussed in appendix A these can be easily obtained by applying the structure-function method. Just in the same way as in the on-shell case the corrections to the off-shell cross-section are calculated by convoluting the lowest-order cross-section (in a certain gauge-invariant scheme) with the appropriate structure functions. In appendix A a detailed analysis is given of the theoretical uncertainties associated with the leading-log procedure.

In the present-day Monte Carlo different ways of implementing the leading logarithmic corrections have been adopted [22]. One method involves solving the evolution equations for the structure functions numerically using techniques known from parton-shower algorithms. In this way soft-photon exponentiation and resummation of the leading logarithms from multiple hard-photon emission are automatically taken into account. Photons are generated according to the matrix elements in the collinear limit, in this way allowing for a finite  $p_T$  kick to the photon. The second method involves a fully inclusive treatment of the radiated photons by folding the improved lowest-order cross-section with leading-log structure functions. So, no explicit photons are generated. The most recent development is a kind of merger of an explicit  $e^+e^- \rightarrow 4f\gamma$  Monte Carlo folded with structure functions, allowing for a consistent definition of observable and unobservable photon radiation (see section 3.4.3).

Another approach is to include the complete ISR. To this end one has to define it in a way that preserves the  $U(1)$  electromagnetic gauge invariance. This is non-trivial because of the presence of the  $t$ -channel diagram which involves a non-conserved charge flow in the initial state. One technique to circumvent this problem is the so-called current-splitting technique [56], which amounts to splitting the electrically neutral neutrino in the  $t$ -channel diagram into two oppositely flowing leptons each with charge one. One of them is attributed to the initial state to build a continuous flow of charge, the other is attributed to the final state to do the same there. The modified  $\nu_e$  propagator leads to additional real and virtual initial-state photonic diagrams which render the ISR gauge-invariant. In this way one obtains the usual universal  $s$ -channel ISR known from LEP1 plus additional non-universal contributions arising from the  $t$ -channel diagrams. The latter are non-factorizing with respect to the lowest-order cross-section, but are screened by a factor  $k_+^2 k_-^2 / s^2$ , which automatically guarantees a unitary behaviour at high energies. Moreover they turn out to be numerically small at LEP2 energies. The universal ISR contains all leading logarithms and can be supplemented by the known universal higher-order terms [57].

It should be noted that both the leading-log and the current-splitting method leave out non-leading photonic corrections, for instance associated with radiation of photons off the intermediate W bosons. For on-shell W bosons we give in table 10 a comparison of exact and leading-log evaluations of the quantity  $\int dE_\gamma E_\gamma (d\sigma/dE_\gamma)$ , needed for the average energy loss

$\sqrt{s}$ [GeV]	$\int dE_\gamma E_\gamma \frac{d\sigma}{dE_\gamma}$ [GeV · pb]	leading-log results		
		$Q^2 = s$ $L$	$Q^2 = s$ $L - 1$	$Q^2 = Q_0^2$ $L - 1$
161.0	$0.1377 \pm 0.0001$	0.1436	0.1379	0.1375
165.0	$3.619 \pm 0.002$	3.792	3.642	3.607
170.0	$10.120 \pm 0.006$	10.651	10.232	10.089
175.0	$17.437 \pm 0.011$	18.431	17.708	17.403
184.0	$30.882 \pm 0.029$	32.873	31.589	30.902
190.0	$39.562 \pm 0.037$	42.224	40.578	39.595
205.0	$59.126 \pm 0.076$	63.581	61.117	59.322

Table 10: The quantity  $\int dE_\gamma E_\gamma (d\sigma/dE_\gamma)$  needed for the average energy loss. The exact on-shell result from hard-photon radiation is given as well as the corresponding leading-log approximation, using  $L = \log(Q^2/m_e^2)$  or  $L - 1$ .

$\langle E_\gamma \rangle$ .<sup>s</sup> It is clear that a sufficiently accurate leading-log evaluation should be based on  $L - 1$  rather than  $L$ . Furthermore, the often-used scale choice  $Q^2 = s$  leads to deviations of about 3% at 190 GeV, which would translate into an error of  $\sim 60$  MeV on  $\langle E_\gamma \rangle$ . The scale choice  $Q_0^2 = 4M_W E/(1 + \beta)$ , however, agrees with the exact result at the 0.3% level for all LEP2 energies, leading to errors below 10 MeV in  $\langle E_\gamma \rangle$ . As there is no obvious reason why these non-leading terms should be smaller in the off-shell case, some care has to be taken with the choice of a suitable leading-log scale.

### 3.4.2 The Coulomb singularity

Another potentially large photonic correction, not associated with the initial state, is due to the Coulomb singularity in the threshold region, which has been discussed for off-shell W-pair production in [58]–[60]. It originates from the IR limit and at one-loop it emerges from a single IR-singular scalar three-point function and a related IR-singular scalar four-point function, the IR-singular part of which is just a scaled version of the one contained in the three-point function (see figure 8). The gauge invariance of the coefficients of these two scalar functions allows us

---

<sup>s</sup>The (lowest-order) average energy loss  $\langle E_\gamma \rangle$  can be obtained by normalizing to the lowest-order cross-section of table 2. Dressing this lowest-order cross-section by LL structure functions, running couplings etc., only makes sense when the energy-weighted cross-section appearing in the numerator is treated in the same way!

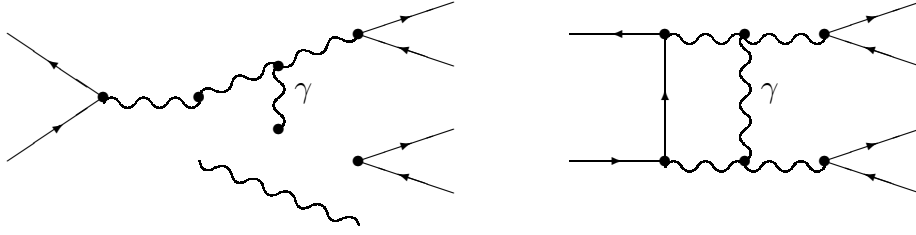


Figure 8: Diagrams that contribute to the Coulomb singularity.

to include the width in a gauge-invariant way. Thus one obtains a gauge-invariant correction factor to the lowest-order cross-section resulting from the doubly-resonant diagrams:

$$\sigma_{\text{Coul}} = \sigma_{\text{Born}}^{\text{CC3}} \frac{\alpha\pi}{2\bar{\beta}} \left[ 1 - \frac{2}{\pi} \arctan \left( \frac{|\beta_M + \Delta|^2 - \bar{\beta}^2}{2\bar{\beta} \text{Im} \beta_M} \right) \right], \quad (60)$$

with

$$\begin{aligned} \bar{\beta} &= \frac{1}{s} \sqrt{s^2 - 2s(k_+^2 + k_-^2) + (k_+^2 - k_-^2)^2}, \\ \beta_M &= \sqrt{1 - 4M^2/s}, \quad M^2 = M_W^2 - iM_W\Gamma_W - i\epsilon, \\ \Delta &= \frac{|k_+^2 - k_-^2|}{s}, \end{aligned} \quad (61)$$

and  $-\pi/2 < \arctan y < \pi/2$ . Here  $\bar{\beta}$  is the average velocity of the W bosons in their centre-of-mass system. Equation (60) only refers to the Coulomb singularity; the finite remnants of the above mentioned three-point function, containing also the IR divergence, have been left out. From equation (60) we obtain the usual on-shell Coulomb singularity for stable W bosons and  $\bar{\beta} \neq 0$  by first going on-shell, i.e.  $\Delta = 0$  and  $\bar{\beta}^2 = \text{Re} \beta_M^2 = \beta^2$ , and subsequently taking the limit  $\Gamma_W \rightarrow 0$ . Note that in this limit the otherwise negligible  $i\epsilon$  in  $M^2$  becomes relevant.

In contrast to the on-shell case there are various effects present in equation (60) that effectively truncate the range of the Coulomb interaction. The presence of a Coulomb singularity requires that  $\bar{\beta}$  be at least of the same order of magnitude as  $\Delta$  and  $|\beta_M|$ , which is bounded by the W width according to  $|\beta_M| \gtrsim \sqrt{\Gamma_W/M_W}$ . This confirms the intuitive argument [58] that the Coulomb singularity is modified substantially by finite-width effects if the characteristic time of the Coulomb interaction ( $t_{\text{Coul}} \sim 1/[\bar{\beta}^2 M_W]$ ) is of the same order as or larger than the typical decay time ( $t_\tau \sim 1/\Gamma_W$ ) of the W bosons. While the effect of the finite W width is contained in  $\beta_M$ , the off-shellness shows up in  $\Delta$  and in the difference  $|\beta_M^2 - \bar{\beta}^2|$ , which effectively involves  $|k_+^2 + k_-^2 - 2M_W^2|/s$ . This is in agreement with the argument [59] that the off-shellness of the virtual W bosons will affect the Coulomb singularity, if the typical times ( $t_{\text{OFS}}^\pm \sim 1/|k_{\pm,0} - \sqrt{M_W^2 + k_\pm^2}| \sim 1/|\sqrt{k_\pm^2} - M_W|$ ) for which off-shell  $W^\pm$  bosons with four-momenta  $k_\pm$  exist is of the same order as or smaller than  $t_{\text{Coul}}$ . It should be noted that as a



result of the convolution with the Breit-Wigner functions from the W resonances, the quantity  $\Delta$  plays a negligible role in an adequate description of the Coulomb phenomenon [59]. Consequently the at first sight deviating formulae of [59] and [60] constitute equally well-justified representations of this phenomenon.

In the case of the total CC3 cross-section, the Coulomb singularity gives rise to a correction factor which reaches its maximal value of  $\sim 5.7\%$  at the nominal threshold and drops smoothly below and above threshold. While it amounts to 2.4% at  $\sqrt{s} = 176$  GeV it is only 1.8% at 190 GeV. The corresponding effect on the reconstructed W mass, resulting from the pronounced energy dependence, is a shift at the level of 5–10 MeV. Because of the fact that the Coulomb singularity is screened by the finite width of the W bosons and the off-shell effects, higher-order Coulomb corrections are not important for off-shell W-pair production [59]–[61]. Moreover, bound states of the two W bosons do not have the time to form because of the finite-width effects. The typical time scale needed for the formation of a bound state  $t_{\text{form}} \sim 1/(\alpha^2 M_W) \approx 234 \text{ GeV}^{-1}$  is much larger than the typical decay time  $t_\tau = 1/\Gamma_W \approx 0.5 \text{ GeV}^{-1}$ .

### 3.4.3 The hard-photon process

As mentioned before, in W-pair production the distinction between initial- and final-state radiation is not unique, unlike in the case of neutral particles such as the Z boson. In the matrix element, the universal leading logarithmic parts are easily separable, but the non-universal finite terms do not split naturally. An accurate calculation of the photon spectrum, beyond the leading logarithmic approximation, thus has to take into account initial-state radiation, final-state radiation, radiation off the W bosons, and various interference effects. These calculations have been performed for the final state consisting of 4 fermions and one photon [62]–[64]. However, the forward emission of many photons, described well by the structure functions and parton-shower algorithms described in section 3.4.1 and in appendix A, is not included in these calculations. Recently efforts have been made to combine the two approaches [65, 66]. We give here the most salient points of these papers.

First we discuss the one-photon matrix element. This contains all graphs with two resonant W propagators, including radiation off the W bosons and the four-vector-boson interaction. The resulting non-leading terms are negative and tend to decrease the energy lost in initial-state radiation. On top of that one can also include the non-doubly-resonant graphs. The universal ones that contribute for all channels are totally negligible [62, 63], just as in the non-radiative process, whereas the  $t$ -channel graphs show the expected collinear  $\log(1 - \cos \theta)$  behaviour.

The next step is to combine this hard matrix element, which is needed for large angles, with the resummed leading-log structure function [65] or parton shower [66], which gives a good description of (multiple-) photon radiation at small angles. This is done by using the exact matrix element (convoluted with initial-state radiation) outside a cone [65] around the incoming

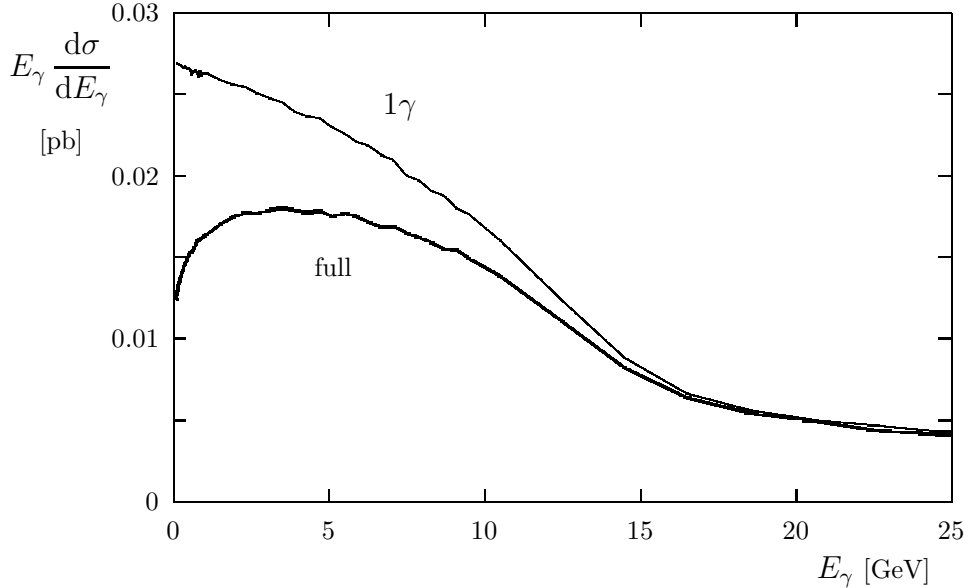


Figure 9: Photon energy spectrum in the one-photon approximation ( $1\gamma$ ) and the same combined with resummed structure functions (full) for the reaction  $e^+e^- \rightarrow \mu^+\nu_\mu\tau^-\bar{\nu}_\tau$ .

electrons and positrons<sup>t</sup>. Inside this cone one subtracts the leading logarithmic contribution from the hard matrix element, adds the tree-level matrix element, and subsequently convolutes everything with initial-state radiation. Of course the structure function or parton shower has to be restricted to radiate within the cone or virtuality cut-off. In the former case the scale  $Q^2 = s(1 - \cos\theta_c)/2$  is used, with  $\theta_c$  defining the cone.

In order to compare this approach with the one-photon matrix element on the one hand, and a purely leading-log description on the other, we have to define some kinematical observables. The most relevant ones for the W-mass measurement are the observable and unobservable photon energies. We define these with respect to the ADLO/TH set of canonical cuts defined in [22]. A photon which passes all cuts is called ‘observable’, and one that is combined with one of the beams is ‘unobservable’. Photons close to final-state particles are not counted either way. The unobservable photon energy is the quantity most relevant to the W-mass reconstruction without explicit photons, whereas the observable photon energy gives an indication how well the resummed leading-log and one-photon matrix elements describe large-angle radiation.

In order to get sensible results for these photon energies we will have to include an estimate of the unresummed soft and virtual corrections, which are not yet fully known. These corrections are only needed inside the cone as a weight of the structure function. As such the corresponding uncertainty partially cancels out in the average photon energies  $\langle E_\gamma \rangle = \int dE_\gamma (d\sigma/dE_\gamma) E_\gamma / \sigma$ . In the actual analysis presented below we circumvent the problem by leaving out the virtual corrections and tuning the non-leading-log part of the soft corrections (through the IR regulator

<sup>t</sup>Instead of a cone also a cut-off on the  $e_{\text{in}}^\pm - \gamma$  virtuality can be used to define the region of multiple-photon radiation [66].

	leptonic	semi-leptonic	hadronic
$\sigma_0$ [pb]	0.712	4.485	7.024
$\sigma_0^{\text{isr}}$ [pb]	0.594	3.732	5.845
$\sigma_{0+\text{bkg}}^{\text{isr}}$ [pb]	0.595	3.736	5.853
$\sigma^{\text{obs}}/\sigma_0^{\text{isr}}$			
full	0.275	0.249	0.229
$1\gamma$	0.365	0.328	0.302
LL	0.286	0.260	0.232
with backgr	0.275	0.250	0.229
$\langle E_\gamma^{\text{obs}} \rangle$ [GeV]			
full	1.227	0.995	0.760
$1\gamma$	1.437	1.167	0.899
LL	1.238	1.028	0.801
with backgr	1.226	0.994	0.759
$\langle E_\gamma^{\text{unobs}} \rangle$ [GeV]			
full	0.676	0.664	0.645
$1\gamma$	0.878	0.873	0.872
LL	0.666	0.667	0.664
with backgr	0.676	0.664	0.644

Table 11: Cross-section for observable photons and the energy lost to observable and unobservable photons at  $\sqrt{s} = 175$  GeV.

mass  $\lambda_{\text{IR}}$ ) in such a way that it cancels in the total cross-section against the non-leading-log part of the hard-photon corrections. Consequently, the resulting total cross-section is simply given by the lowest-order cross-section convoluted with leading logarithmic structure functions. As the initial-final and final-final interference is expected to be of order  $\alpha\Gamma_W/M_W$  (see section 3.4.4), this is a reasonable approximation.

The results for the structure-function algorithm of [65] are given in table 11 for leptonic, semi-leptonic, and hadronic final states<sup>u</sup>. For the cone  $\theta_c = 10^\circ$  was chosen, but the results do not depend strongly on this parameter ( $\theta_c = 5^\circ$  only shifts the values by about 1%). In table 11 we first give the observable tree-level non-radiative doubly-resonant cross-section ( $\sigma_0$ ), the same convoluted with leading-log structure functions ( $\sigma_0^{\text{isr}}$ ), and with in addition the universal non-doubly-resonant (background) graphs ( $\sigma_{0+\text{bkg}}^{\text{isr}}$ ). For the next entries we consider the

<sup>u</sup>It should be noted that only the universal background diagrams were taken into account.

full calculation described above, the exact one-photon matrix element ( $1\gamma$ ), and the leading-log result (LL). We also give the full result including the universal non-doubly-resonant diagrams (full+backgr). The statistical errors on the cross-sections are  $\mathcal{O}(0.1\%)$ , but the differences (LL – full) and ((res + backgr) – res) were computed directly in this form and have relative errors of a few per cent and a few tens of per cent, respectively, on these differences. The statistical errors on the average photon energies are slightly larger, 0.3–0.5%. Note that we introduced an upper cut-off on the photon energy to avoid the Z peak. This influences only the observable average energy.

One can see that an appreciable fraction (around one quarter) of the events will be accompanied by photons observable in the ADLO/TH set of cuts. This is due to the excellent forward coverage ( $\theta_\gamma > 1^\circ$ ) and electromagnetic calorimeter ( $E_\gamma > 0.1$  GeV) assumed in the canonical cuts. Reducing the angle to  $10^\circ$  this fraction still is around 20%, half of which also has an  $E_\gamma > 1$  GeV. Neither the  $1\gamma$  matrix element nor the leading-log approximation give a satisfactory description of the observable photons. By radiating only one photon one misses the additional convolution with the structure functions, which scales down the one-photon cross-section as a result of the large, negative soft-photon effects. On the other hand, the leading-log approximation misses the negative effects from initial–final state interference and the radiation off the intermediate W bosons. Finally, given that the un-exponentiated large-angle contribution of the cross-section still is 20% of the total cross-section, the  $E_\gamma$  spectrum in the region  $E_\gamma < 1$  GeV should not be trusted to 1%, even not in the full calculation. Most of the cross-section here is, however, associated with the final state and hence does not influence the W-mass measurement.

The observable photon energy is dominated by final-state radiation and hence not very interesting. The unobservable energy spectrum is much more independent of the specific final state. It is not completely independent due to the possibility of observable jets in the beam pipe (there is no angular cut on jets in the canonical cuts). The initial-state radiation associated with these events is sometimes combined with the final state by the canonical cuts, thus lowering the average energy. As the radiation off jets is not modelled correctly anyway, a jet-angle cut will have to be imposed to exclude this contamination. One sees that analysing observable photons separately reduces the average energy loss, and hence the size of the theoretical corrections to be applied to the fitted W-mass. For the unobservable radiation the leading-log approximation is, as expected, quite good. Like in the total cross-section, the contribution of the universal non-doubly-resonant graphs is negligible.

We conclude that the one-photon matrix element does not describe observable photons or unobservable photons well, whereas a leading logarithmic description is not accurate enough for large-angle photons, as it does not include the negative contributions associated with interference terms and radiation off the W bosons. Furthermore, a separate analysis of the events with an observable photon (around one quarter of all events with the canonical cuts) reduces the average energy loss considerably, thus reducing the uncertainties coming from this theoretical input.

### 3.4.4 General approach to radiative corrections within the pole scheme

Finally, we discuss the way in which a reasonable approximation to the full radiative corrections to the process  $e^+e^- \rightarrow 4f$  can be computed. We do not consider QCD corrections. The perturbative QCD corrections to the final state are well-understood, as the main part is confined to the decay of a single  $W$ , which should be similar to the hadronic  $Z$  decays studied at LEP1. Perturbative QCD interference effects between the decay products of different  $W$  bosons are suppressed by a factor  $\alpha_s^2/(N_C^2 - 1)$ . The related non-perturbative interference effects associated with the hadronization are discussed in section 3.5.

An electroweak  $\mathcal{O}(\alpha)$  calculation would consist of the traditional three parts: one-loop graphs, soft-photon bremsstrahlung, and hard-photon bremsstrahlung. Only the sum is IR finite. The separation between hard and soft radiation is, as usual, defined with respect to a photon-energy cut-off  $E_{\min}^\gamma$ . Because of the finite  $W$  width one either has to use  $E_{\min}^\gamma \ll \Gamma_W$  to ensure the validity of the soft-photon approximation in the soft-bremsstrahlung integrals (i.e., neglecting the effect of the photon momentum on the phase space and on the non-IR-singular parts of the matrix element), or one has to take into account finite photon energies in the Breit-Wigner resonances. Close to threshold, moreover, the limited amount of available phase space demands  $E_{\min}^\gamma \ll M_W \beta^2$ .

The soft-bremsstrahlung integrals factorize into a simple multiplicative factor and the Born amplitude, and can easily be added, either using a ‘fixed-width scheme’ or the ‘fermion-loop scheme’. Hard-photon radiation (for an arbitrary cut-off) has already been addressed in section 3.4.3.

What remains are the virtual corrections. However, the full one-loop calculation of the virtual diagrams appears daunting. For the most simple final state,  $e^+e^- \rightarrow \mu^+\nu_\mu\bar{u}d$ , there are 3579 Standard-Model Feynman diagrams for massless fermions. This increases to 7158 when one electron is included in the final state, and reaches 15948 for the most complicated final state  $e^+e^- \nu_e \bar{\nu}_e$ . However, not all contributions are equally important. For instance the numerical significance of the non-doubly-resonant (background) diagrams is small in the Born and hard-photon calculations, especially if one requires that the event resembles  $W$ -pair production. So, we can assume that the one-loop corrections to these diagrams are even smaller. The problem then amounts to achieve a clean separation of the radiative corrections to  $W$ -pair production.

One way to achieve this separation is the ‘pole scheme’ introduced in section 3.3 for tree-level matrix elements. There have been various attempts to define one-loop corrections in this scheme [23]–[25], which differ considerably. Since so far no actual calculation for  $W$ -pair production has been completed in such a scheme, we restrict ourselves to a few comments. The idea behind the ‘pole scheme’ is to include a minimal part of the higher-order corrections needed to generate a finite width. By making a systematic expansion both in the coupling parameter  $\alpha$  and in the width  $\Gamma$  ( $\propto \alpha$ ), one can identify gauge-invariant contributions of progressively smaller influence on the final result. We will roughly sketch the method for a single, neutral particle. For factorizable diagrams, i.e. diagrams that factorize into corrections

to the production, propagation, and decay of the unstable particles, the amplitude to all orders can be Dyson resummed as follows [24, 67]

$$\begin{aligned} \mathcal{M}_{\text{fact}}^{\infty} &= \frac{W(p^2, \theta)}{p^2 - m^2} \sum_{n=0}^{\infty} \left( \frac{\Sigma(p^2)}{p^2 - m^2} \right)^n = \frac{W(p^2, \theta)}{p^2 - m^2 - \Sigma(p^2)} \\ &= \left[ \frac{W(p^2, \theta)}{p^2 - m^2 - \Sigma(p^2)} - \frac{W(M^2, \theta)}{p^2 - M^2} \frac{1}{1 - \Sigma'(M^2)} \right] + \frac{W(M^2, \theta)}{p^2 - M^2} \frac{1}{1 - \Sigma'(M^2)}, \quad (62) \end{aligned}$$

where  $m$  denotes the real mass, and  $M$  the complex mass given by  $M^2 - m^2 - \Sigma(M^2) = 0$ . The corrections to production and decay are contained in the function  $W$ , and  $\Sigma(p^2)$  is the one-particle-irreducible self-energy. The variable  $\theta$  in the vertex-correction function  $W$  stands for other variables, which have to be chosen sensibly (see section 3.3). The first term of equation (62) does not have a pole and the residue at the pole  $p^2 = M^2$  of the last term is gauge-invariant. In [25] it has been shown how to derive the single-pole residue  $W(M^2, \theta)/[1 - \Sigma'(M^2)]$  and the non-pole terms. The former consists essentially of the on-shell amplitude plus some terms of  $\mathcal{O}(\Gamma)$ . It should, however, be noted that this type of decomposition only works when the on-shell limit exists. So, for instance below the  $W$ -pair production threshold the ‘pole-scheme’ method makes no sense, and as a result of that the procedure is not reliable just above threshold.

When one turns to the production of charged unstable particles, additional problems arise related to the infra-red divergences that occur in the limit  $\Gamma \rightarrow 0$ . Again these problems can be overcome [25, 9].

So far the above discussion only took into account factorizable diagrams. There are also non-factorizable diagrams, e.g. diagrams in which a photon connects the initial and final state or the decay products of different unstable particles. Those non-factorizable diagrams can give rise to double-pole contributions when the virtual photon becomes soft. Combined with the related soft bremsstrahlung it has been shown that the non-factorizable double-pole contributions cancel up to order  $\alpha\Gamma/m$  in the fully inclusive total cross-section [69, 70]. For sufficiently exclusive distributions this is in general not the case [9, 70, 71].

### 3.5 Reconnection effects

Nearly half of all  $W$  pairs decay hadronically. In the LEP2 energy range the average space-time distance between the  $W^+$  and  $W^-$  decay vertices is smaller than 0.1 fm, i.e. less than a typical hadronic size of 1 fm. Therefore the fragmentation of the  $W^+$  and the  $W^-$  may not be independent, and this could influence the  $W$ -mass reconstruction. Here a short summary of the problem is given in a historical order. More can be found in the report of the  $W$ -mass group [8].

The problem is related to two different physical effects: colour reconnections and Bose-Einstein effects.

The colour-reconnection problem was first pointed out in [72] using the string-model approximation. Assuming that the  $W$  pair decays into two quark-antiquark pairs  $q\bar{q}$  and  $Q\bar{Q}$ , respectively, it can either fragment into two strings stretched between  $q\bar{q}$  and  $Q\bar{Q}$ , or into two strings stretched between  $q\bar{Q}$  and  $\bar{q}Q$ . In the three-colour world the probability for the second configuration was taken to be  $1/9$  in a very crude approximation. The properties of these two configurations are very different. While the first one gives ‘classical’ event multiplicities and a flat rapidity distribution, the second one has a small multiplicity and the particles are grouped at large rapidity values [72].

The fragmentation of the initial  $q\bar{q}$  pairs into hadrons is conventionally described in terms of a perturbative parton cascade followed, at a later stage, by a non-perturbative hadronization phase. In perturbative QCD (PQCD) the influence of one  $W$  fragmentation on the other one is called ‘interconnection’. Here the timing is very important [8, 73]: the gluon-emission time of high-energy gluons,  $\tau_g \sim 1/E_g$ , is shorter than the  $W$  lifetime,  $\tau_W \sim 1/\Gamma_W \approx 0.5 \text{ GeV}^{-1}$ . Therefore the gluons with  $E_g \gg \Gamma_W$  are emitted independently from the  $q\bar{q}$  and  $Q\bar{Q}$  systems, while gluons with  $E_g \leq \Gamma_W$  may feel four colour charges ( $\Rightarrow$  PQCD interference) [73]. The non-perturbative hadronization (at distances  $\sim 1 \text{ fm}$ ) is NOT independent. The influence of PQCD interference is shown to be not very important [73, 74]. It is suppressed by a colour factor  $1/(N_C^2 - 1) = 1/8$  as compared to the total rate of double primary gluon emission and, in addition, only gluons with  $E_g \leq \Gamma_W$  are concerned; thus the total suppression factor is about 100 compared to a naive instantaneous reconnection scenario with all events reconnected. It is much more complicated to estimate the influence of the fragmentation effects. In the Lund string model analogies to two types of superconductors have been used [73]. The reconnection probability is taken to be either proportional to the space–time volume over which the  $W^+$  and  $W^-$  strings overlap (type I superconductor) or to the probability that vortex lines cross (type II superconductor). Using these models the fragmentation error was estimated to be 30 MeV on the  $W$ -mass measurement. This error is increased to 40 MeV by adding the estimated error coming from the perturbative effects as well as from the interplay between perturbative and non-perturbative effects. Also an extended version of this approach has been investigated [8], where additionally the space–time evolution of the parton cascade, multiple reconnections, and a finite vortex-core radius have been taken into account.

In [75] the space–time picture is not used, except for the timing of the gluon emission. Rather it is assumed that reconnections reducing the total string length are preferred, as indicated by PQCD experience. During fragmentation, in addition to the standard string connections between quarks and gluons emitted from each  $W$ , also any other possible interconnection (recoupling) between partons emitted from different  $W$  bosons is possible with a probability that may be very different from  $1/9$ . The reduced string length leads to a reduction in multiplicity in the central rapidity region. In this model the shift in the reconstructed  $W$ -mass varies between 6 and 60 MeV (‘shortest-string’ version) or between 13 and 130 MeV (‘random-reconnection’ version) if the recoupling probability varies between 10 and 100%. Methods to measure this probability using data from LEP2 have been suggested [8, 75]. A similar model has been introduced in the ARIADNE program leading to similar mass shifts [76].

The preliminary estimate of the colour reconnection in HERWIG, based on a reduction of the space-time extent of clusters, gives mass shifts of the same order as the ones mentioned above [8].

The dependence of the shift in the reconstructed W-mass on the parameters of different models has been studied by the LEP experiments in more details [8]. It appears that uncertainties using experimental procedures are not smaller than the ones obtained above. The issue whether diagnostic signals for reconnection can be found is still open.

Thus the colour-reconnection effect may add a big systematic error to the W-mass measurement in the four-quark channel. The interesting aspect is that different approaches give uncertainties of the same order.

It may be worthwhile to note that similar (but not identical) ‘unconventional’ colour connections can also appear inside a single Z system, as is discussed in [8]. The presence/absence of a signal in Z decays at LEP1 could give an indication of the expected effects in the  $W^+W^-$  system.

Bose–Einstein correlations have been observed experimentally as an enhancement in the two-particle correlation function for identical bosons. In the case of a W pair decaying hadronically a possibility exists of Bose–Einstein correlations between particles that come from different W bosons [77]. A test of this effect has been made in a model based on PYTHIA and JETSET [77]. The model gives large reconstructed positive mass shifts of the order of 100 MeV, rising with increasing c.m.s. energy and with decreasing source radius. The real shift may be smaller due to various damping factors not included in [77] (which is intended as a ‘worst-case’ scenario), but effects of the order of 50 MeV could be expected within a large class of possible Bose–Einstein models.

In the coming years both colour (re)arrangement and Bose–Einstein effects can and should be studied both theoretically and experimentally. Also the large statistics collected already at LEP1 may help to study both these effects.

## 4 Concluding Remarks

In this report the present status of the theoretical knowledge of W-pair production and the related process of four-fermion production is reviewed.

In lowest-order complete evaluations for all four-fermion final states exist, taking into account all Feynman diagrams. The theoretical problem how to incorporate an energy-dependent width in the W and Z propagators without spoiling gauge invariance has been solved for the lowest-order cross-section. The numerical relevance of imposing electromagnetic gauge invariance is explicitly demonstrated.



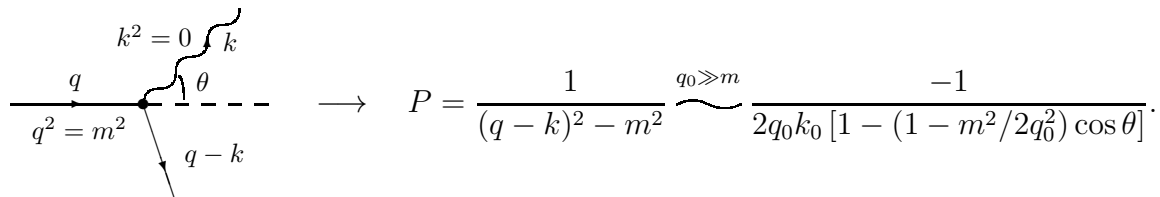
As to the radiative corrections, the state of the art depends on whether on- or off-shell  $W$ -pair production, or four-fermion production is considered. Complete  $\mathcal{O}(\alpha)$  RC's only exist for on-shell  $W$ -pair production. The dominant RC's that can be taken into account properly for all three types of processes comprise leading-log ISR, the leading weak effects related to  $G_\mu$  and  $\alpha(s)$ , and the Coulomb singularity. The  $\mathcal{O}(\alpha)$  RC's for four-fermion production obviously do not exist, and can at best be calculated using approximative techniques. Only taking along the above dominant effects, the total and differential cross-sections at 175 and 190 GeV are estimated to be known at the 1–2% level (based on on-shell experience). For the total cross-section at 161 GeV an uncertainty of about 2% is expected. Part of the latter uncertainty is due to the possible variation of the Higgs mass. This Higgs-mass dependence is largest for light Higgs bosons and is most pronounced at threshold.

Another question, relevant for the reconstruction of the  $W$  mass, is the accuracy of the average emitted photon energy  $\langle E_\gamma \rangle$ . At 175 and 190 GeV a precision of 10–20 MeV seems feasible, provided a proper scale is used in the structure-function part of the calculation.

## A Various Methods of Calculating QED Corrections

### A.1 The structure-function method

As pointed out in the previous sections, the virtual and real corrections reveal the presence of large logarithmic QED effects of the form  $\alpha L/\pi \equiv (\alpha/\pi) \log(Q^2/m_e^2)$  with  $Q^2 \gg m_e^2$ . They arise when photons or light fermions are radiated off in the direction of incoming or outgoing light particles [78, 79], provided the momentum of the latter is kept fixed (exclusive) [79]. In a massless theory these large logarithms would show up as collinear divergences (like in QCD), but in the SM the masses of the particles act as natural cut-offs. The fact that they can nevertheless give rise to sizeable corrections is due to the difference in scale between the mass of the radiating particle and its energy. This is illustrated by considering the propagator  $P$  of a light particle after photon emission



$$\begin{array}{c}
 \begin{array}{c}
 \text{---} \xrightarrow{q} \text{---} \text{---} \xrightarrow{k} \text{---} \text{---} \\
 \text{---} \xrightarrow{q-k} \text{---} \\
 \theta \\
 \text{---} \text{---} \text{---}
 \end{array}
 \quad \longrightarrow \quad
 P = \frac{1}{(q-k)^2 - m^2} \overset{q_0 \gg m}{\sim} \frac{-1}{2q_0 k_0 [1 - (1 - m^2/2q_0^2) \cos \theta]}
 \end{array}$$

In the limit  $m \rightarrow 0$  this propagator gives rise to a pole at  $\cos \theta = 1$ . For finite  $m$  it yields large logarithmic terms of the form  $\log(q_0^2/m^2)$  when the photon momentum is integrated over (inclusive photon). A consequence of the direct relation between the large QED logarithms and collinear divergences is that they are controlled by renormalization group equations and that they are universal, i.e. they are process-independent. They can be calculated using the so-called structure-function method [16], taken over from QCD. This procedure also allows the inclusion of soft-photon effects to all orders by means of exponentiation.

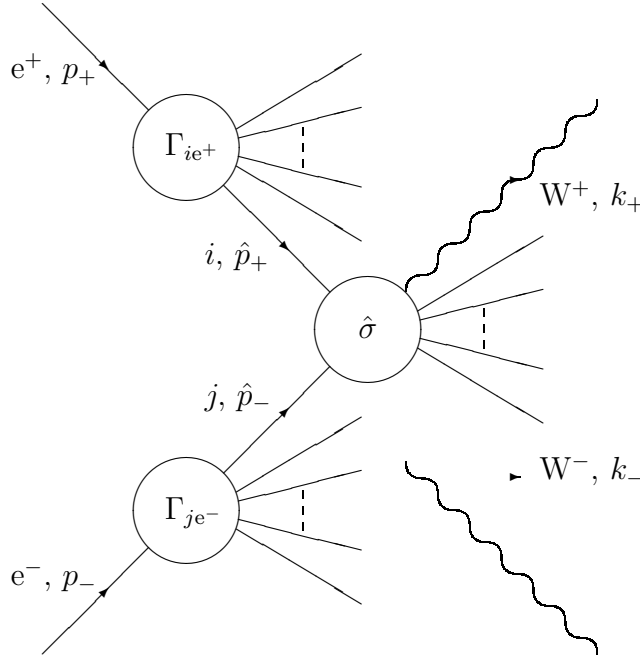


Figure 10: Initial-state collinear radiation in  $e^+e^- \rightarrow W^+W^-$ . The unlabeled external lines represent an arbitrary number of undetected (inclusive) particles.

The structure-function method is based on the mass-factorization theorem (see figure 10):

$$s^4 \frac{d^4 \sigma_{e^+e^- \rightarrow W^+W^-X}}{dt_1 du_1 dt_2 du_2} = \int_0^1 \frac{dx_+}{x_+^2} \int_0^1 \frac{dx_-}{x_-^2} \Gamma_{ie^+}(x_+, Q^2) \Gamma_{je^-}(x_-, Q^2) \hat{s}^4 \frac{d^4 \hat{\sigma}_{ij \rightarrow W^+W^-X'}}{d\hat{t}_1 d\hat{u}_1 d\hat{t}_2 d\hat{u}_2}(Q^2), \quad (63)$$

which links the cross-section  $\sigma_{e^+e^- \rightarrow W^+W^-X}$ , where X indicates an arbitrary number of undetected particles, to the hard scattering cross-section  $\hat{\sigma}_{ij \rightarrow W^+W^-X'}$  which is free of the large collinear logarithms<sup>v</sup>. The indices  $i, j$  represent all light-particle transitions allowed by QED (e.g.  $\gamma, e^\pm, \mu^\pm, \dots$ ). Furthermore we have defined

$$\begin{aligned} t_1 &\equiv (p_- - k_-)^2 - M_W^2, & u_1 &\equiv (p_+ - k_-)^2 - M_W^2, \\ t_2 &\equiv (p_+ - k_+)^2 - M_W^2, & u_2 &\equiv (p_- - k_+)^2 - M_W^2. \end{aligned} \quad (64)$$

Analogously their hatted counterparts are given by the same expressions with  $p_\pm$  replaced by  $\hat{p}_\pm = x_\pm p_\pm$ . It should be noted that (63) allows the implementation of various cuts on the energies and angles of the produced W bosons, and that it can be used to extract more commonly used distributions [like  $d\sigma/(d\cos\theta_+)$ ] by supplying the appropriate Jacobians [80]. The

---

<sup>v</sup>If the final state consists of exclusively treated light particles (e.g.  $e^+e^- \rightarrow 4f$ ), large collinear final-state QED logarithms appear. These large logs can be treated in a way similar to the initial-state ones, provided proper account is taken of the fact that now  $\hat{p} = p/x$ .

structure functions  $\Gamma_{ij}$  describe ‘mass singular’ initial-state collinear radiation and represent the probability of finding in the parent particle  $j$  at the scale  $Q^2$  a particle  $i$  with fraction  $x$  of longitudinal momentum. So  $(1-x)$  denotes the fraction of energy carried away by collinear radiation. All large collinear logarithms are contained in the structure functions, which depend, just like the hard scattering cross-section, on the mass-factorization scale  $Q^2$ . These structure functions can be decomposed into a part containing the collinear logarithms and a non-log part according to

$$\begin{aligned}\Gamma_{ij}^{\text{log}}(x, Q^2) &= \delta_{ij} \delta(1-x) + \sum_{n=1}^{\infty} \left(\frac{\alpha}{\pi}\right)^n \sum_{m=1}^n a_{mn}^{ij}(x) L^m, \\ \Gamma_{ij}^{\text{non-log}}(x, Q^2) &= \sum_{n=1}^{\infty} \left(\frac{\alpha}{\pi}\right)^n b_n^{ij}(x).\end{aligned}\tag{65}$$

Analogously the hard scattering cross-section can be decomposed into the scale-independent Born cross-section plus non-log higher-order terms

$$d\hat{\sigma}_{ij}(Q^2) = d\sigma_{ij}^{\text{Born}} + \sum_{n=1}^{\infty} \left(\frac{\alpha}{\pi}\right)^n c_n^{ij}(Q^2).\tag{66}$$

For convenience we have dropped the explicit dependence on  $x_{\pm}$  in this decomposition. This dependence enters via the reduced momenta  $\hat{p}_{\pm}$ .

The so-called leading-log (LL) approximation consists in only taking along the terms  $\propto (\alpha L/\pi)^n$ , which automatically means that the hard scattering cross-section  $\hat{\sigma}$  should be identical to the scale-independent Born cross-section. In addition this Born cross-section could be dressed by the leading corrections that are not of the LL type, e.g. running couplings or a Coulomb factor, in order to improve the approximation. As these LL contributions constitute the most important higher-order QED effects, it is on most occasions sufficient to add the  $\mathcal{O}(\alpha^2)$  LL contributions to the full  $\mathcal{O}(\alpha)$  results and to exponentiate the soft-photon distribution. In this way the resulting cross-section becomes scale-dependent. A further simplification can be achieved by realizing that in  $e^+e^-$  collisions the bulk of the QED corrections frequently originates from pure photon radiation, especially when the soft-photon contributions are dominant<sup>w</sup>.

After these simplifications the relevant structure function takes on the form [81, 82]

$$\begin{aligned}\Gamma_{ee}^{\text{LL,exp}}(x, Q^2) \equiv \phi(\alpha, x, Q^2) &= \frac{\exp(-\frac{1}{2}\gamma_E \beta_{\text{exp}} + \frac{3}{8}\beta_S)}{\Gamma(1 + \frac{1}{2}\beta_{\text{exp}})} \frac{\beta_{\text{exp}}}{2} (1-x)^{\beta_{\text{exp}}/2-1} - \frac{1}{4}\beta_H (1+x) \\ &\quad - \frac{1}{4^2 2!} \beta_H^2 \left[ \frac{1+3x^2}{1-x} \log(x) + 4(1+x) \log(1-x) + 5+x \right] \\ &\quad - \frac{1}{4^3 3!} \beta_H^3 \left\{ (1+x) \left[ 6 \text{Li}_2(x) + 12 \log^2(1-x) - 3\pi^2 \right] \right\}\end{aligned}$$

---

<sup>w</sup>For more details concerning polarized structure functions and QED corrections that are not of the pure-photon-radiation type we refer to [9].

$$\begin{aligned}
& + \frac{1}{1-x} \left[ \frac{3}{2} (1 + 8x + 3x^2) \log(x) + 6(x+5)(1-x) \log(1-x) \right. \\
& \left. + 12(1+x^2) \log(x) \log(1-x) - \frac{1}{2} (1+7x^2) \log^2(x) + \frac{1}{4} (39 - 24x - 15x^2) \right] \Big\}. \quad (67)
\end{aligned}$$

Here  $\text{Li}_2(y)$  is the dilogarithm,  $\gamma_E$  the Euler constant, and  $\Gamma(y)$  the Gamma function (not to be confused with the structure functions). In terms of this structure function the total W-pair production cross-section including exponentiated LL QED corrections can for example be written as

$$\sigma_{\text{LL,exp}}(s, Q^2) = \int_{4M_W^2/s}^1 dz \phi(2\alpha, z, Q^2) \hat{\sigma}_0(zs), \quad (68)$$

where  $\hat{\sigma}_0(zs)$  denotes the (possibly improved) Born cross-section at the reduced CM energy squared  $zs$ .

Note that some non-leading terms can be incorporated, taking into account the fact that the residue of the soft-photon pole is proportional to  $L - 1$  rather than  $L$  for the initial-state photon radiation. Using

$$\eta = \frac{2\alpha}{\pi} L \quad \text{and} \quad \beta = \frac{2\alpha}{\pi} (L - 1) \quad (69)$$

we can identify a couple of popular options for including non-leading terms:

- $\beta_{\text{exp}} = \beta$ ,  $\beta_S = \beta_H = \eta$  [9, 83] (‘MIXED’ choice)
- $\beta_{\text{exp}} = \beta_S = \beta$ ,  $\beta_H = \eta$  [84] (‘ETA’ choice); the original Gribov–Lipatov form factor [85]
- $\beta_{\text{exp}} = \beta_S = \beta_H = \beta$  [56, 86] (‘BETA’ choice).

The differences between these options are in the coefficient in front of the exponentiated soft-photon term and in the use of  $\eta$  or  $\beta$  in the hard parts.

In table 12 we quantify for the CC3 process  $e^+e^- \rightarrow W^+W^- \rightarrow 4f$  the uncertainty associated with these three different structure functions. We give the total cross-section without cuts, the radiative energy loss  $\langle E_\gamma \rangle$ , and the invariant-mass loss  $\langle M_\gamma \rangle$ . The radiative energy loss is defined as

$$\langle E_\gamma \rangle = \frac{1}{\sigma} \int (2 - x_+ - x_-) E d\sigma \quad (70)$$

and the radiative invariant-mass loss as

$$\langle M_\gamma \rangle = \frac{1}{\sigma} \int (1 - x_+ x_-) E d\sigma. \quad (71)$$

As can be seen from the comparison between the third and fourth column of table 12, the effect on the total cross-section due to the different coefficient in front of the exponentiated soft-photon term in the MIXED and ETA structure functions is of the order of 0.3–0.4%. This

$\sqrt{s}$ [GeV]		MIXED to $\mathcal{O}(\beta^2)$	ETA to $\mathcal{O}(\beta^2)$	BETA to $\mathcal{O}(\beta^2)$	BETA to $\mathcal{O}(\beta^3)$
175	$\sigma$	13.2218(11)	13.1772(12)	13.1828(13)	13.1790(11)
	$\langle E_\gamma \rangle$	1.1120(3)	1.1115(3)	1.1147(3)	1.1146(3)
	$\langle M_\gamma \rangle$	1.1093(3)	1.1090(3)	1.1120(3)	1.1119(3)
190	$\sigma$	16.3412(8)	16.2829(12)	16.2969(13)	16.2939(8)
	$\langle E_\gamma \rangle$	2.1303(4)	2.1300(5)	2.1395(5)	2.1391(4)
	$\langle M_\gamma \rangle$	2.1220(4)	2.1216(5)	2.1314(5)	2.1314(4)
205	$\sigma$	17.1302(17)	17.0696(12)	17.0897(17)	17.0869(13)
	$\langle E_\gamma \rangle$	3.1823(9)	3.1817(9)	3.2011(9)	3.2019(7)
	$\langle M_\gamma \rangle$	3.1666(10)	3.1655(9)	3.1845(10)	3.1854(9)

Table 12: Effects of different structure functions on  $\sigma$  (in pb),  $\langle E_\gamma \rangle$  (in GeV), and  $\langle M_\gamma \rangle$  (in GeV), for the CC3 process  $e^+e^- \rightarrow W^+W^- \rightarrow 4f$ .

different choice in the coefficient does not affect  $\langle E_\gamma \rangle$  and  $\langle M_\gamma \rangle$ , since it is a factorized soft-photon contribution which largely cancels out in the ratios. By comparing the fourth and fifth column of table 12, one can estimate the amount of the so-called  $\eta \rightarrow \beta$  effect in the hard part of the structure function. The impact on the cross-section is small, i.e. of the order of 0.1% (depending on the energy). The effect on  $\langle E_\gamma \rangle$  and  $\langle M_\gamma \rangle$  is 3, 10, 19 MeV (at  $\sqrt{s} = 175, 190, 205$  GeV, respectively) and therefore not significant in view of the expected experimental accuracy at LEP2. From the last two columns of table 12, finally, we can infer that the effects of the  $\mathcal{O}(\beta^3)$  hard part of the structure function is completely negligible.

At this point we would like to note that the leading effects related to the production of undetected  $e^+e^-$  pairs from conversion of a virtual photon emitted from the initial state (+ corresponding loop corrections) can be accounted for by replacing  $\alpha$  in  $\phi(\alpha, x, Q^2)$  by  $\alpha[1 + \alpha L/(6\pi)]$ . This takes into account the QED  $\beta$ -function contributions appearing in the renormalization group equations. Also other fermion pairs can be included, but care has to be taken with the fact that the real pair-production process requires the virtual photon to be sufficiently hard.

Another source of uncertainties is related to the fact that the scale  $Q^2$  is a free parameter<sup>x</sup>. As mentioned already in section 2.3.3, all ‘natural’ scale choices are roughly equal close to threshold. Hence, when using the structure-function method to calculate higher-order corrections [beyond  $\mathcal{O}(\alpha)$ ] the  $Q^2$  dependence is negligible. This is, of course, not the case for LL  $\mathcal{O}(\alpha)$  corrections, as they are larger. So, in situations where the exact  $\mathcal{O}(\alpha)$  corrections are not known and one has to resort to a LL approximation instead, as is the case for  $e^+e^- \rightarrow 4f$ , the scale dependence is larger.

---

<sup>x</sup>For a discussion of ‘appropriate’ scale choices we refer to [9].

## A.2 The parton-shower method

The basic assumption of the QED parton-shower method is that the structure function of an electron (or positron) obeys the Altarelli–Parisi equation [87], which can be expressed by the integral equation

$$\Gamma_{ee}(x, Q^2) = \Pi_{ee}(Q^2, Q_s^2) \Gamma_{ee}(x, Q_s^2) + \frac{\alpha}{2\pi} \int_{Q_s^2}^{Q^2} \frac{dK^2}{K^2} \Pi_{ee}(Q^2, K^2) \int_x^{1-\epsilon} \frac{dy}{y} P_{ee}(y) \Gamma_{ee}(x/y, K^2) \quad (72)$$

in the leading-log approximation [88]. Here  $\epsilon$  is a small quantity specified later and  $P_{ee}(x) = (1+x^2)/(1-x)$ . The function  $\Pi_{ee}$ , which is nothing but the Sudakov factor, is given by

$$\Pi_{ee}(Q^2, Q'^2) = \exp \left[ -\frac{\alpha}{2\pi} \int_{Q'^2}^{Q^2} \frac{dK^2}{K^2} \int_0^{1-\epsilon} dx P_{ee}(x) \right], \quad (73)$$

and denotes the probability that the electron (or positron) evolves from  $Q'^2$  to  $Q^2$  without emitting a hard photon. The scale  $Q_s^2$  is, like in appendix A.1, a free parameter (of order  $m_e^2$ ). Often it is chosen such that, when the  $K^2$  dependence is integrated out, the factor  $\beta$  emerges rather than  $\eta$ .

Equation (72) can be solved by iterating the right-hand side in a successive way. Hence it is apparent that the emission of  $n$  photons corresponds to the  $n$ -th iteration. As such it is possible to regard the process as a stochastic one, suggesting the following algorithm for the photon shower [89]: (a) Set  $x_b = 1$ . The variable  $x_b$  is the fraction of the light-cone momentum of the virtual electron (or positron) that annihilates. (b) Choose a random number  $\xi$ . If it is smaller than  $\Pi_{ee}(Q^2, Q_s^2)$ , then the evolution stops. If not, one proceeds by finding the virtuality  $K^2$  that satisfies  $\xi = \Pi_{ee}(K^2, Q_s^2)$ . With this virtuality a branching takes place. (c) Fix  $x$  according to the probability  $P_{ee}(x)$  between 0 and  $1 - \epsilon$ . Then  $x_b$  is replaced by  $x_b x$ . Subsequently one should go to (b), replacing  $Q_s^2$  by  $K^2$ , and repeat until the evolution stops.

Once an exclusive process is fixed by this algorithm, each branching of a photon in the process is dealt with as a true process, that is, an electron with  $x, K^2$  decays as  $e^-(x, -K^2) \rightarrow e^-(xy, -K'^2) + \gamma(x[1-y], Q_0^2)$ . Here  $Q_0^2$  is a cut-off to avoid the IR divergence. It is unphysical, so any physical observable should not depend on it. The momentum conservation at the branching gives  $-K^2 = -K'^2/y + Q_0^2/(1-y) + \mathbf{k}_T^2/(y[1-y])$ , which in turn determines  $\mathbf{k}_T^2$  from  $y, K^2, K'^2$ . Hence the  $\mathbf{k}_T^2$  distribution can be taken into account in the simulation as well as the shape of  $x$ . This feature represents the essential difference between the structure-function method, which treats the photons inclusively, and the QED parton-shower method. Keeping in mind that  $y \leq 1 - \epsilon$ , the kinematical boundary  $y(K^2 + Q_0^2/[1-y]) \leq K'^2$ , equivalent to  $\mathbf{k}_T^2 > 0$ , fixes  $\epsilon$  to  $\epsilon = Q_0^2/K^2$ , since strong ordering ( $K^2 \ll K'^2$ ) is expected.

The above description of the algorithm represents the “single-cascade scheme”. This implies that only the  $e^-$  or the  $e^+$  is able to radiate photons when the axial gauge vector is chosen along the momentum of the other initial-state particle, namely  $e^+$  or  $e^-$ . For programming purposes, however, it is convenient to use a symmetrization procedure (the so-called “double-cascade

scheme”) to ensure the symmetry of the radiation with respect to the electron and positron [90, 91]. The so-obtained QED parton shower can then be combined with the matrix element of any hard process initiated by  $e^+e^-$  annihilation.

The Altarelli–Parisi equations can also be solved by a different algorithm [92], which yields equivalent results for electromagnetic radiative corrections.

Starting from the observation that the most important corrections come from multiple soft-photon emission, the photon-number distribution can be approximated by a Poisson distribution with average photon number

$$\bar{n}_\gamma = \frac{\alpha}{2\pi} \log\left(\frac{Q^2}{m_e^2}\right) \int_0^{1-\epsilon} dx P_{ee}(x). \quad (74)$$

The technical infra-red cut-off  $\epsilon$  will drop out of the physical sum over soft photons. After the number of photons has been chosen from the Poisson distribution, their transverse and longitudinal momenta can be generated properly, ordered according to the  $1/(p_\pm \cdot k)$  poles and splitting functions, respectively.

Using momentum conservation at each branching, the correct energy loss and  $p_T$  boost for the hard scattering is obtained. This algorithm has been shown to yield results that are consistent with the structure-function formalism and provides a realistic approximation for the photonic  $\mathbf{k}_T^2$  distributions.

### A.3 YFS exponentiation

Let us first answer the basic question: what the exclusive Yennie–Frautschi–Suura (YFS) exponentiation *is* and what it *is not*? YFS exponentiation *is*, in one word, a technique of summing up all IR singularities for a given arbitrary process to infinite order. The formal proof in [68] is based on Feynman-diagram techniques and goes ‘order by order’. The YFS technique *is not* by any means bound to the leading-log summation technique and/or approximations. It *is* applicable to arbitrary stable particles (with arbitrary mass and spin) in the initial and final state. The YFS summation is inherently exclusive, i.e. all subtractions/summations of IR-singular contributions are done *before* any phase-space integrations over virtual- or real-photon four-momenta are performed. This means that the Monte Carlo technique can be used to integrate over the multiple real-photon phase space. The first practical solution of this kind was given in [93]. Here the QED matrix element that enters the YFS exponentiation consists of two parts. The  $\mathcal{O}(\alpha)$  part is taken to be exact, i.e. from Feynman diagrams, whereas a LL approximation is used to write down an economic ansatz for the  $\mathcal{O}(\alpha^2)$  part. The YFS-exponentiation procedure, which involves a subtraction of the IR part of the matrix element, knows nothing about the origin of the matrix element (ansatz or Feynman rules), and it will fail if the ansatz has the wrong IR limit. The above subtraction procedure is done on the fully differential distribution *before* phase-space integration. Hence it should be clear that a LL ansatz for the matrix element in which the emitted photons have zero transverse momenta *is not possible*.

Contrary to the LL techniques described in appendices A.1 and A.2, in the YFS approach the parameter  $\beta = 2(\alpha/\pi)[\log(s/m_e^2) - 1]$  results from the integration over phase space and there is no freedom to adjust it. There is no discussion “do we have  $-1$  in the definition of the leading logarithm or not”. The  $-1$  is mandatory, because otherwise the IR singularities do not cancel. The orthodox YFS exponentiation technique [68] is essentially ‘order by order’ and as such it *does not* sum up all the LL corrections to infinite order, something which is in principle possible for the LL techniques described in appendices A.1 and A.2.

As the exact  $\mathcal{O}(\alpha)$  matrix element for  $e^+e^- \rightarrow 4f$  is not yet known, the present implementation of YFS exponentiation for this process relies on a pure LL ansatz [94]. But this will, of course, change as soon as an adequate approximative  $\mathcal{O}(\alpha)$  calculation becomes available.

## References

- [1] S.L. Glashow, *Nucl. Phys.* **22** (1961) 579;  
S. Weinberg, *Phys. Rev. Lett.* **19** (1967) 1264;  
A. Salam, in *Elementary Particle Theory*, ed. N. Svartholm (Almqvist and Wiksells, Stockholm, 1968), p. 367;  
S.L. Glashow, J. Iliopoulos and L. Maiani, *Phys. Rev.* **D2** (1970) 1285.
- [2] A. Olshevsky, talk presented at the International Europhysics Conference on High Energy Physics, Brussels, Belgium, 27/7–2/8 1995.
- [3] W. Hollik, talk presented at the XV Int. Conference on Physics in Collisions, Cracow, Poland, June 1995, hep-ph/9507406.
- [4] P. Gambino and A. Sirlin, *Phys. Rev.* **73** (1994) 621;  
Z. Hioki, *Phys. Lett.* **B340** (1994) 181;  
S. Dittmaier et al., *Nucl. Phys.* **B426** (1994) 249; **E: B446** (1995) 334;  
F. Jegerlehner, in *Physics at LEP200 and Beyond*, eds. J. Blümlein and T. Riemann (North-Holland, Amsterdam, 1994), p. 129.
- [5] UA2 Collaboration, J. Alitti et al., *Phys. Lett.* **B276** (1992) 354;  
CDF Collaboration, F. Abe et al., *Phys. Rev. Lett.* **75** (1995) 11; *Phys. Rev.* **D52** (1995) 4784;  
D0 Collaboration, preliminary results presented by C.K. Jung, talk given at the 27th ICHEP, Glasgow, Scotland, 20–27 July 1994.
- [6] D. Bardin, W. Hollik and G. Passarino (eds.), *Reports of the working group on precision calculations for the Z resonance* (CERN-95-03, Geneva, 1995).
- [7] CDF Collaboration, F. Abe et al., *Phys. Rev. Lett.* **74** (1995) 2626;  
D0 Collaboration, S. Abachi et al., *Phys. Rev. Lett.* **74** (1995) 2632.



- [8] The contribution of the working group *Determination of the mass of the W boson*, this report.
- [9] W. Beenakker and A. Denner, *Int. J. Mod. Phys.* **A9** (1994) 4837.
- [10] The contribution of the working group *Triple gauge boson couplings*, this report.
- [11] K. Hagiwara et al., *Nucl. Phys.* **B282** (1987) 253.
- [12] M. Bilenky et al., *Nucl. Phys.* **B409** (1993) 22.
- [13] C.P. Burgess and D. London, *Phys. Rev. Lett.* **69** (1992) 3428, *Phys. Rev.* **D48** (1993) 4337;  
G.J. Gounaris and F.M. Renard, *Z. Phys.* **C59** (1993) 133;  
C. Grosse-Knetter, I. Kuss and D. Schildknecht, *Z. Phys.* **C60** (1993) 375;  
F. Boudjema, in *Physics and Experiments with Linear  $e^+e^-$  Colliders*, eds. F.A. Harris et al. (World Scientific, Singapore, 1993), Vol. II, p. 712.
- [14] M. Böhm et al., *Nucl. Phys.* **B304** (1988) 463;  
W. Beenakker, K. Kołodziej and T. Sack, *Phys. Lett.* **B258** (1991) 469;  
W. Beenakker, F.A. Berends and T. Sack, *Nucl. Phys.* **B367** (1991) 287.
- [15] J. Fleischer, F. Jegerlehner and M. Zralek, *Z. Phys.* **C42** (1989) 409;  
K. Kołodziej and M. Zralek, *Phys. Rev.* **D43** (1991) 3619;  
J. Fleischer, F. Jegerlehner and K. Kołodziej, *Phys. Rev.* **D47** (1993) 830.
- [16] E.A. Kuraev and V.S. Fadin, *Sov. J. Nucl. Phys.* **41** (1985) 466;  
G. Altarelli and G. Martinelli, in *Physics at LEP*, eds. J. Ellis and R. Peccei (CERN-86-02, Geneva, 1986), Vol. 1, p. 47.
- [17] W.J. Marciano and D. Wyler, *Z. Phys.* **C3** (1979) 181;  
D. Albert et al., *Nucl. Phys.* **B166** (1980) 460;  
K. Inoue et al., *Prog. Theo. Phys.* **64** (1980) 1008;  
T.H. Chang, K.J.F. Gaemers and W.L. van Neerven, *Nucl. Phys.* **B202** (1982) 407.
- [18] F. Jegerlehner, *Z. Phys.* **C32** (1986) 425 and in *Proc. of the 11th International School of Theoretical Physics 'Testing of the Standard Model'*, Szczyrk-Bila (Poland) 1987, eds. M. Zralek and R. Manka (World Scientific, Singapore, 1988), p. 127.
- [19] D.Yu. Bardin, S. Riemann and T. Riemann, *Z. Phys.* **C32** (1986) 121.
- [20] A. Denner and T. Sack, *Z. Phys.* **C46** (1990) 653.
- [21] T. Muta, R. Najima and S. Wakaizumi, *Mod. Phys. Lett.* **A1** (1986) 203.
- [22] The contribution of the working group *Event generators for WW physics*, this report.
- [23] M. Veltman, *Physica* **29** (1963) 186.

- [24] R.G. Stuart, *Phys. Lett.* **B262** (1991) 113.
- [25] A. Aeppli, G.J. van Oldenborgh and D. Wyler, *Nucl. Phys.* **B428** (1994) 126.
- [26] Particle Data Group, *Phys. Rev.* **D50** (1994) 1173.
- [27] S. Eidelman and F. Jegerlehner, *Z. Phys.* **C67** (1995) 585;  
H. Burkhardt and B. Pietrzyk, *Phys. Lett.* **B356** (1995) 398.
- [28] W.J. Marciano, *Phys. Rev.* **D29** (1984) 580.
- [29] V. Barger, T. Han and R.J.N. Phillips, *Phys. Rev.* **D39** (1989) 146;  
H. Tanaka, T. Kaneko and Y. Shimizu, *Comp. Phys. Commun.* **64** (1991) 149;  
E.N. Argyres et al., *Phys. Lett.* **B259** (1991) 195.
- [30] A. Sommerfeld, *Atombau und Spektrallinien*, (Vieweg, Braunschweig, 1939), Bd. 2;  
A.D. Sakharov, *JETP* **18** (1948) 631.
- [31] W. Beenakker and G.J. van Oldenborgh, in preparation.
- [32] S. Dittmaier, M. Böhm and A. Denner, *Nucl. Phys.* **B376** (1992) 29; E: **B391** (1993) 483.
- [33] J. Fleischer et al., *Nucl. Phys.* **B378** (1992) 443.
- [34] M. Consoli, W. Hollik and F. Jegerlehner, *Phys. Lett.* **B227** (1989) 167;  
M. Consoli, W. Hollik and F. Jegerlehner, in *Z physics at LEP 1*, eds. G. Altarelli, R. Kleiss and C. Verzegnassi (CERN-89-08, Geneva, 1989), Vol. 1, p. 7;  
W. Hollik, Lectures at the CERN-JINR School of Physics 1989, Egmond-aan-Zee, Netherlands, in CERN-91-07 (1991).
- [35] A. Djouadi and C. Verzegnassi, *Phys. Lett.* **B195** (1987) 265;  
A. Djouadi, *Nuovo Cimento* **100A** (1988) 357;  
B.A. Kniehl, *Nucl. Phys.* **B347** (1990) 86;  
F. Halzen and B.A. Kniehl, *Nucl. Phys.* **B353** (1991) 567.
- [36] L. Avdeev et al., *Phys. Lett.* **B336** (1994) 560; E: **B349** (1995) 597;  
K.G. Chetyrkin, J.H. Kühn and M. Steinhauser, *Phys. Lett.* **B351** (1995) 331.
- [37] J. van der Bij and F. Hoogeveen, *Nucl. Phys.* **B283** (1987) 477.
- [38] R. Barbieri et al., *Phys. Lett.* **B288** (1992) 95; E: **B312** (1993) 511;  
R. Barbieri et al., *Nucl. Phys.* **B409** (1993) 105.
- [39] G. Degrassi et al., in *Reports of the working group on precision calculations for the Z resonance*, eds. D. Bardin, W. Hollik and G. Passarino (CERN-95-03, Geneva, 1995), p. 163.

- [40] A. Denner, *Fortschr. Phys.* **41** (1993) 307.
- [41] D. Bardin et al., in *Physics at LEP200 and Beyond*, eds. J. Blümlein and T. Riemann (North-Holland, Amsterdam, 1994), p. 148.
- [42] F.A. Berends, R. Kleiss and R. Pittau, *Nucl. Phys.* **B424** (1994) 308.
- [43] D. Bardin and T. Riemann, DESY preprint DESY 95–167, to appear in *Nucl. Phys. B*.
- [44] A. Aeppli, F. Cuyper and G.J. van Oldenborgh, *Phys. Lett.* **B314** (1993) 413.
- [45] U. Baur, J.A.M. Vermaseren and D. Zeppenfeld, *Nucl. Phys.* **B375** (1992) 3.
- [46] Y. Kurihara, D. Perret-Gallix and Y. Shimizu, *Phys. Lett.* **B349** (1995) 367.
- [47] U. Baur and D. Zeppenfeld, *Phys. Rev. Lett.* **75** (1995) 1002.
- [48] H. Simma, 1991, private communication.
- [49] W. Beenakker, in  *$e^+e^-$  Collisions at 500 GeV: The Physics Potential*, ed. P.M. Zerwas (DESY 92–123, Hamburg, 1992), part A, p. 195.
- [50] C.G. Papadopoulos, *Phys. Lett.* **B352** (1995) 144.
- [51] E.N. Argyres *et al.*, *Phys. Lett.* **B358** (1995) 339.
- [52] E.N. Argyres *et al.*, in preparation.
- [53] J. Papavassiliou and A. Pilaftsis, hep-ph/9507246.
- [54] A. Denner, S. Dittmaier and G. Weiglein, *Phys. Lett.* **B333** (1994) 420.
- [55] F.A. Berends and G.B. West, *Phys. Rev.* **D1** (1970) 122.
- [56] D. Bardin et al., *Phys. Lett.* **B308** (1993) 403; E: hep-ph/9507277.
- [57] F.A. Berends, G. Burgers and W.L. van Neerven, *Phys. Lett.* **B185** (1987) 395; *Nucl. Phys.* **B297** (1988) 429; E: **B304** (1988) 921.
- [58] V.S. Fadin, V.A. Khoze and A.D. Martin, *Phys. Lett.* **B311** (1993) 311.
- [59] D.Yu. Bardin, W. Beenakker and A. Denner, *Phys. Lett.* **B317** (1993) 213.
- [60] V.S. Fadin et al., *Phys. Rev.* **D52** (1995) 1377.
- [61] V.A. Khoze and T. Sjöstrand, hep-ph/9508332.
- [62] A. Aeppli and D. Wyler, *Phys. Lett.* **B262** (1991) 125.
- [63] G.J. van Oldenborgh, P.J. Franzini, and A. Borrelli, *Comp. Phys. Commun.* **83** (1994) 14.

- [64] J. Fujimoto et al., in *Physics at LEP200 and Beyond*, eds. J. Blümlein and T. Riemann (North-Holland, Amsterdam, 1994), p. 169.
- [65] G.J. van Oldenborgh, Leiden preprint INLO-PUB-95/04, 1995.
- [66] J. Fujimoto et al., in preparation.
- [67] H. Veltman, *Z. Phys.* **C62** (1994) 35.
- [68] D.R. Yennie, S.C. Frautschi and H. Suura, *Ann. of Phys.* **13** (1961) 379.
- [69] V.S. Fadin, V.A. Khoze and A.D. Martin, *Phys. Rev.* **D49** (1994) 2247.
- [70] K. Melnikov and O. Yakovlev, hep-ph/9501358.
- [71] V.S. Fadin, V.A. Khoze and A.D. Martin, *Phys. Lett.* **B320** (1994) 141;  
K. Melnikov and O. Yakovlev, *Phys. Lett.* **B324** (1994) 217.
- [72] G. Gustafson, U. Pettersson and P.M. Zerwas, *Phys. Lett.* **B209** (1988) 90.
- [73] T. Sjöstrand and V.A. Khoze, *Z. Phys.* **C62** (1994) 281; *Phys. Rev. Lett.* **72** (1994) 28.
- [74] E. Accomando, A. Ballestrero and E. Maina, *Phys. Lett.* **B362** (1995) 141.
- [75] G. Gustafson and J. Häkkinen, *Z. Phys.* **C64** (1994) 659.
- [76] L. Lönnblad, CERN preprint CERN-TH/95-218.
- [77] L. Lönnblad and T. Sjöstrand, *Phys. Lett.* **B351** (1995) 293.
- [78] N. Nakanishi, *Prog. Theo. Phys.* **19** (1958) 159.
- [79] T. Kinoshita, *J. Math. Phys.* **3** (1962) 650;  
T.D. Lee and M. Nauenberg, *Phys. Rev.* **133** (1964) B1549.
- [80] W. Beenakker, F.A. Berends and W.L. van Neerven, in *Radiative Corrections for  $e^+e^-$  Collisions*, ed. J.H. Kühn (Springer, Berlin Heidelberg, 1989), p. 3.
- [81] F.A. Berends et al., in *Z physics at LEP 1*, eds. G. Altarelli, R. Kleiss and C. Verzegnassi (CERN-89-08, Geneva, 1989), p. 89.
- [82] M. Skrzypek and S. Jadach, *Z. Phys.* **C49** (1991) 577;  
M. Skrzypek, *Acta Physica Polonica* **B23** (1992) 135;  
M. Cacciari et al., *Europhysics Letters* **17** (1992) 123.
- [83] F.A. Berends, R. Kleiss and R. Pittau, *Nucl. Phys.* **B426** (1994) 344.
- [84] G. Montagna et al., *Phys. Lett.* **B348** (1995) 178.
- [85] V.N. Gribov and L.N. Lipatov, *Sov. J. Nucl. Phys.* **15** (1972) 438, 675.

- [86] G. Montagna, O. Nicrosini and F. Piccinini, *Comp. Phys. Commun.* **90** (1995) 141.
- [87] G. Altarelli and G. Parisi, *Nucl. Phys.* **B126** (1977) 298.
- [88] R. Odorico, *Nucl. Phys.* **B172** (1980) 157;  
G. Marchesini and B.R. Webber, *Nucl. Phys.* **B238** (1984) 1.
- [89] J. Fujimoto, Y. Shimizu and T. Munehisa, *Prog. Theo. Phys.* **90** (1993) 177, *ibid.* **91** (1994) 333.
- [90] T. Munehisa et al., KEK–CP–034, KEK preprint 95–114, 1995.
- [91] K. Kato and T. Munehisa, *Phys. Rev.* **D39** (1989) 156.
- [92] H.D. Dahmen et al., *Z. Phys.* **C50** (1991) 75;  
H. Anlauf et al., *Comp. Phys. Commun.* **79** (1994) 487;  
H. Anlauf et al., in *Physics at LEP200 and Beyond*, eds. J. Blümlein and T. Riemann (North-Holland, Amsterdam, 1994), p. 81.
- [93] S. Jadach and B.F.L. Ward, *Comp. Phys. Commun.* **56** (1990) 351.
- [94] M. Skrzypek et al., CERN preprint CERN–TH/95–205, to appear in *Comp. Phys. Commun.*